issn 0065-3713

INSTITUT D'AERONOMIE SPATIALE DE BELGIQUE

3 - Avenue Circulaire
B - 1180 BRUXELLES

AERONOMICA ACTA

A - N° 381 - 1994

Thresholds for magnetic percolation through the magnetopause current layer in asymmetrical magnetic fields

by

M.M. Kuznetsova and M. Roth

BELGISCH INSTITUUT VOOR RUIMTE-AERONOMIE

3 - Ringlaan
B - 1180 BRUSSEL

FOREWORD

This paper has been accepted for publication in *Journal of Geophysical Research (Space Physics)*

AVANT–PROPOS

Cet article a été accepté comme publication dans le *Journal of Geophysical Research (Space Physics)*

VOORWOORD

Dit artikel is aanvaard voor publikatie in *Journal of Geophysical Research (Space Physics)*

VORWORT

Dieser Aufsatz wird in *Journal of Geophysical Research (Space Physics)* erscheinen

Thresholds for Magnetic Percolation through the Magnetopause Current Layer in Asymmetrical Magnetic Fields

M.M. Kuznetsova * and M. Roth§

Abstract

The Vlasov kinetic approach is used to study the stability of magnetic surfaces with respect to spontaneous excitation of collisionless tearing perturbations within magnetopause current layers (MCLs) with asymmetrical magnetic field profiles. For the unperturbed configuration a "tractable" (that is, with a minimum number of free parameters) Vlasov equilibrium model describing a tangential discontinuity is developed. In this model, asymmetrical MCLs are not electrostatically equipotential configurations and their structure is only determined by the angle of the magnetic field rotation θ_0 and the magnetic field asymmetry factor $\kappa_B = (B_2 - B_1)/B_2$, where B_1 and B_2 are the magnetic field intensities in the adjacent magnetosheath and magnetospheric regions, respectively. The stochastic percolation model by Galeev et al. (1986), based on the symmetrical charge-neutral Harris equilibrium, is generalized for asymmetrical MCLs. Asymmetry in the **B** field profile strongly modifies the dependence of the marginal MCL thickness (below which the MCL is subjected to percolation) on the polarity of the interplanetary magnetic field (IMF). For a northward IMF ($\theta_0 < 90°$), the percolation is impossible when $\kappa_B \geq 0.4$, while for moderate values of κ_B ($0.15 \leq \kappa_B < 0.4$) only thin MCLs can be percolated. When $\kappa_B > 0.3$, the maximum thickness of MCLs subjected to percolation is achieved for $\theta_0 > 90°$, that is, for a southward IMF. Assuming that the magnetopause should, on the average, be close to its stability threshold, realistic asymmetrical MCLs (with $\kappa_B > 0.3$) should be thinner for a northward IMF than for a southward IMF.

Résumé

Pour étudier la stabilité des surfaces magnétiques de la magnétopause par rapport à l'excitation spontanée de perturbations de type "tearing" non collisionnelles, au sein de couches de courant (MCLs) caractérisées par des profils asymétriques du champ ma-

*Space Research Institute, Russian Academy of Sciences
Profsoyuznaya 84/32, R-117810 Moscow, Russia. *Now at:*
Laboratory for Extraterrestrial Physics, NASA/GSFC
Greenbelt, MD 20771, USA.

§*Institut d'Aéronomie Spatiale de Belgique*
Avenue Circulaire 3, B-1180 Brussels, Belgium.

gnétique, nous avons utilisé une approche cinétique basée sur l'équation de Vlasov. Pour décrire la configuration non perturbée, un modèle d'équilibre simplifié—de type Vlasov—(avec un nombre minimum de paramètres libres) a été développé. Dans ce modèle, les couches de courant asymétriques représentant la magnétopause (MCLs) ne sont pas, d'un point de vue électrostatique, des configurations équipotentielles, et leurs structures sont uniquement déterminées par l'angle de rotation du champ magnétique θ_0 et par le facteur d'asymétrie du champ magnétique κ_B ($\kappa_B = (B_2 - B_1)/B_2$, où B_1 et B_2 sont les intensités du champ magnétique dans les régions adjacentes ; respectivement la magnétogaine et la magnétosphère).

Le modèle stochastique de percolation de Galeev et al. (1986) basé sur le modèle d'équilibre de Harris (symétrique et électrostatiquement neutre) a été généralisé aux cas de couches MCLs asymétriques. L'asymétrie du profil du champ **B** modifie fortement la dépendance de l'épaisseur marginale de la MCL (en deçà de laquelle la MCL est soumise à une percolation) par rapport à la polarité du champ magnétique interplanétaire (IMF). Lorsque le champ IMF possède une orientation nord ($\theta_0 < 90°$), la percolation est impossible si $\kappa_B \geq 0.4$; tandis que pour des valeurs modérées de κ_B ($0.15 \leq \kappa_B < 0.4$), seules des MCLs minces peuvent être l'objet de percolation. Lorsque $\kappa_B > 0.3$, l'épaisseur marginale des MCLs est maximale pour $\theta_0 > 90°$, c'est-à-dire, pour une orientation sud du champ IMF. Considérant que la magnétopause devrait, en moyenne, être proche de son seuil de stabilité, les MCLs avec des facteurs d'asymétrie réalistes ($\kappa_B > 0.3$) devraient être plus minces lorsque le champ IMF est orienté au nord, plutôt qu'au sud.

Samenvatting

Een kinetisch model gebaseerd op de Vlasov vergelijking wordt gebruikt om de stabiliteit voor spontaan opgewekte botsingsvrije verbrokkelingsverstoringen ("collisionless tearing perturbations") van magnetische grenslagen te onderzoeken. Dit wordt gedaan voor stroomlagen in de magnetopause (MCLs), die worden gekenmerkt door een asymmetrisch magnetisch veld profiel. Het niet-verstoorde regime wordt bestudeerd aan de hand van een Vlasov evenwichtsmodel dat een tangentiële discontinuïteit beschrijft met een minimaal aantal parameters. In dit model zijn asymmetrische MCLs geen elektrostatische equipotentiaal-configuraties; hun structuur wordt uitsluitend bepaald door de rotatiehoek θ_0 van het magnetisch veld, en door de asymmetrie-factor κ_B ($\kappa_B = (B_2 - B_1)/B_2$, waarin B_1 en B_2 de magnetische veldsterkten voorstellen in de magnetoschede en de magnetosfeer, aan weerszijden van de MCL).

Het stochastische percolatie-model beschreven door Galeev et al. (1986), dat gebaseerd is op de symmetrische neutrale evenwichtstoestand volgens Harris, wordt hier veralgemeend voor asymmetrische MCLs. Asymmetrie in het **B**-profiel beïnvloedt in sterke mate de relatie tussen de marginale dikte van de MCL (beneden dewelke percolatie door de MCL mogelijk is) en de polariteit van het interplanetair magnetisch veld (IMF). Voor een IMF met noord-polariteit ($\theta_0 < 90°$) is percolatie onmogelijk wanneer $\kappa_B \geq 0.4$, terwijl voor gematigde waarden van κ_B ($0.15 \leq \kappa_B \leq 0.4$) enkel percolatie door dunne MCLs plaatsvindt. Wanneer $\kappa_B > 0.3$ wordt de maximale dikte van de MCL voor dewelke percolatie nog optreedt, bereikt voor $\theta_0 > 90°$, dit wil zeggen, een IMF met zuid-polariteit. In de veronderstelling dat de dynamica van de magnetopause doorgaans dicht bij de stabili-

teitsgrens ligt, moeten realistische asymmetrische MCLs (met $\kappa_B > 0.3$) dunner zijn voor een IMF met noord-polariteit dan voor een IMF met zuid-polariteit.

Zusammenfassung

Um die Stabilität der magnetischen Flächen der Magnetopause im Verhältnis zur spontanen Erregung von "tearing"–artigen stoßfreien Störungen in, mit asymetrische Profile des Magnetfeldes, Stromschichten der Magnetopause (MCL) zu untersuchen, wählten wir einen auf die Vlasov'sche Gleichung gegründeten kinetischen Ansatz. Zur Beschreibung der nichtgestörten Konfiguration wurde ein vereinfachtes Vlasov–artiges Gleichgewichtsmodell mit einer Mindestanzahl freier Parameter die die tangentiale Diskontinuität beschreiben entwickelt. In diesem Modell sind die die Magnetopause (MCL) darstellenden asymetrischen Stromschichten — elektrostatisch gesehen — keine äquipotentialen Konfigurationen und ihre Strukturen werden lediglich durch den Rotationswinkel des Magnetfeldes θ_0 und durch den Asymetriefaktor des Magnetfeldes κ_B ($\kappa_B = (B_2 - B_1)/B_2$), bestimmt, wobei B_1 und B_2 die Intensitäten des Magnetfeldes in den anliegenden Bereichen darstellen, d.h. die Magnethülle respektive die Magnetosphäre. Das auf dem symetrisch und elektrostatisch neutralem Gleichgewichtsmodell nach Harris beruhende stochastische Perkolationsmodell von Galeev und al. (1986) wurde auf die Fälle asymetrischer MCL–Schichten verallgemeinert. Die Asymetrie des **B**–Feld–Profils verursacht eine bedeutsame Abhängigkeit der MCL–Grenzdicke (unterhalb derer die MCL einer Perkolation unterliegt) in bezug auf die Polarität des interplanetären Magnetfeldes (IMF). Ist das IMF–Feld nach Norden orientiert ($\theta_0 < 90°$), so ist bei $\kappa_B \geq 0.4$ die Perkolation unmöglich; während bei mässigen κ_B–Werten ($0.15 \leq \kappa_B < 0.4$) nur dünne MCL eine Perkolation erfahren. Wenn $\kappa_B > 0.3$, ist die maximale Dicke der MCLs bei $\theta_0 > 90°$, d.h. bei einer Orientierung des IMF–Feldes nach Süden maximal. Davon ausgehend, das durchschnittlich die Magnetopause ihrer Stabilitätßchwelle nahe kommen dürfte, müßten die MCL mit realistischen Asymetriefaktoren ($\kappa_B > 0.3$) bei nördlicher eher als bei südlicher IMF–Feldorientierung dünner sein.

1 Introduction

Study of the structure and dynamics of transition current layers separating two magnetized plasmas with different characteristics is of fundamental importance in understanding various phenomena in laboratory and space. Magnetopause current layers (MCLs) are formed at outer boundaries of planetary magnetospheres where the solar wind is stopped and deflected by a strong intrinsic magnetic field. The simplest model of a planetary MCL is described by a tangential discontinuity within which the magnetic field rotates from an arbitrary interplanetary direction to a magnetospheric direction. Statistical studies of abundant experimental material show, however, that interplanetary and geomagnetic field lines sometimes are topologically connected. The discovery of flux transfer events (FTEs) at the Earth's magnetopause [*Russell and Elphic*, 1978, 1979] indicates that this connection of magnetic field lines can be spatially and temporally localized. Although alternative explanations for FTEs phenomena have been put forward by *Lemaire and Roth* [1991], *Roth* [1992], and *Sibeck* [1992], the transient reconnection nature of FTEs is widely discussed in the literature.

The discovery of FTEs has given an impulse to the development of unsteady and patchy reconnection models. Most of these theoretical models have been proposed to explain the phenomenon of FTEs (see, for example, *Lee and Fu* [1985], *Pudovkin and Semenov* [1985], *Galeev et al.* [1986], *Scholer* [1988], *Hesse et al.* [1990], *Tetreault* [1992], *Lee et al.* [1993], and references cited in these works). In this domain a considerable amount of papers decribes MHD simulations of the dayside magnetic driven reconnection (see, for example, *Fu and Lee* [1985], *Sato et al.* [1986], *Shi et al.* [1988], *Ogino et al.* [1989], *Otto* [1990], *Shi and Lee* [1990], *Fu et al.* [1990], *Ding et al.* [1991], *Liu et al.* [1992]). In some of these MHD simulations the effect of different initial parameters on both sides of the MCL was analyzed (see, for example, *Hoshino and Nishida* [1983], *La Belle-Hamer et al.* [1988], *Scholer* [1989], *Pu et al.* [1990]). The MHD models are focused on the global structure of FTEs without addressing the resistivity mechanism responsible for reconnection. The assumed spatial and temporal variations of resistivity may, however, not be realistic in the collisionless magnetospheric plasma. Microscopic plasma turbulence in the magnetopause region plays an important role and could act as an effective resistivity. Microturbulence is indeed observed to be a permanent feature of magnetopause crossings [e.g., *Gurnett et al.*, 1979; *Gary and Eastman*, 1979; *LaBelle and Treumann*, 1988]; *Tsurutani et al.*, 1989; and references therein]. The observed amplitude of the most intense turbulence is of the order of few millvolt per meter. The lower hybrid drift instability is considered as the most plausible candidate to explain these oscillations when the interplanetary magnetic field is northward [*Gary and Eastman*, 1979; *Sotnikov et al.*, 1981; *Gary and Sgro*, 1990]. However, for significant angles between the magnetosheath and magnetospheric magnetic fields the strong stabilizing influence of the magnetic shear on the lower hybrid drift instability [*Krall*, 1977; *Huba et al.*, 1982; *Gladd et al.*, 1985] could be very important, but this topic requires further studies. Recent work has shown that an anomalous resistivity can be associated with the destabilization of whistlers [J. F. Drake et al., The structure of thin current layers: Implications for magnetic reconnection, submitted to *Journal of Geopysical Research,* 1994] or with the current convective instability in small-scale current

structures (with transverse scale lengths smaller than the electron skin depth) embedded in the broader magnetopause current layer [*Drake et al.*, 1994].

Many advances have also been made in particle simulations of collisionless magnetic reconnection [*Ding et al.*, 1992b; and references therein]. Another group of papers based on the kinetic Vlasov formalism invokes a specific reconnection mechanism: collisionless drift tearing modes [*Laval et al.*, 1966; *Galeev and Zelenyi*, 1977; *Coppi et al.*, 1979; *Quest and Coroniti*, 1981; *Galeev et al.*, 1986; *Kuznetsova and Zelenyi*, 1985, 1990a, b; *Gladd*, 1990]. The main advantage of the kinetic approach is that it does not require an "ad hoc" resistivity and describes spontaneous processes driven by the free energy of the MCL magnetic field itself. This approach is more appropriate for investigating the fine dynamics of thin current layers (a few ion Larmor radii thickness). This analytical (or semianalytical) approach allows us to obtain a parametric dependence of the reconnection process and helps us to make a deeper insight into the physics of the problem. The main difficulty in the framework of the one-dimensional kinetic Vlasov approach is to include self-consistently some elements of the global pattern.

The linear and nonlinear dynamics of the collisionless drift tearing mode has been thoroughly investigated by *Galeev and Zelenyi* [1977], *Coppi et al.* [1979], *Kuznetsova and Zelenyi* [1985, 1990a, b]. The stochastic percolation model based on these studies has been suggested by *Galeev et al.* [1986]. It will hereafter be referred to as the GKZ model. In this model reconnection was considered as an irregular multiscale process associated with the magnetic field diffusion caused by the self-consistently generated magnetic turbulence. This stochastic process results in the formation of magnetic field lines connecting both sides of the current layer via an irregular path. The necessary condition for the magnetic percolation through the MCL appears to be the destruction of all magnetic surfaces within it. This condition imposes a bound on the thickness of the MCL for the formation of reconnection "patches" with characteristic spatial scales along the magnetopause $\lambda_z \times \lambda_y$. The marginal thickness depends on the angle of the magnetic field rotation θ_0, the single factor characterizing the difference between conditions on both sides of the equilibrium MCL used in the GKZ model. Results of particle simulations of magnetic field line stochasticity due to the growth and overlapping of multiple tearing mode islands within such a symmetrical current layer reported recently by *Wang and Ashour-Abdalla* [1994] support the GKZ percolation model.

In the GKZ model (as well as in many other papers devoted to this subject, for example, *Drake and Lee* [1977], *Galeev and Zelenyi* [1977], *Coppi et al.* [1979], *Quest and Coroniti* [1981], *Gladd* [1990], *Wang and Ashour-Abdalla* [1994]) the well-known *Harris* [1962] configuration (generalized for the case where the plasma is magnetized by the constant current-aligned magnetic field component B_y) was chosen as an initial equilibrium structure

$$\mathbf{B} = B_0 \tanh(X/L)\mathbf{e_z} + B_y\mathbf{e_y}, \quad B_y = \text{const} \tag{1}$$

This magnetic field configuration describes the main property of the MCL, the rotation of the magnetic field vector across the layer, the angle of rotation being $\theta_0 = 2\ \text{arctg}(B_0/B_y)$. Configuration (1) corresponds to a symmetrical MCL composed of a population of trapped particles "isolated" from the magnetosheath and magnetospheric plasmas. The latter can only be introduced self-consistently in the form of an uniform background with a constant

number density n_b [*Kuznetsova and Zelenyi*, 1990b]

$$n(X)=n_0\cosh^{-2}(X/L)+n_b,\ 8\pi n_0(T_e+T_i)=B_0^2 \tag{2}$$

Observations show however that the magnetopause is a mixture of plasmas of both magnetosheath and magnetospheric origins [*Bryant and Riggs*, 1989]. Layers with a constant or nearly constant value of B_y are seldom observed and the field magnitude clearly increases in the earthward direction. The violation of the "B_y=const" approximation appears to be especially important for small values of the magnetic field shear ($B_0 < B_y$, $\theta_0 < 90°$), when the pressure balance condition in (2) is unlikely satisfied, because the plasma may now be confined not only by the "azimuthal" field $B_0(X)$, but also by the weak gradient of the "guiding" field B_y. The less the angle θ_0 the more pronounced this effect. To avoid this difficulty *Galeev et al.* [1986] modified the equilibrium constraint in (2) in the following way

$$8\pi n_0(T_e+T_i) = B_0^2 + \alpha B_y^2 \tag{3}$$

where the parameter α characterizes the role of a current-aligned magnetic field in the magnetopause plasma confinement. For $\theta_0 < 90°$ the results of the stability analysis appears to be very sensitive to the choice of α (that is, to the choice of the initial configuration). For $\alpha = 1$ (when the maximum kinetic pressure $n_0(T_e + T_i)$ is assumed to be equal to the maximum magnetic pressure $(B_0^2 + B_y^2)/8\pi$) $\theta_0 = 60°$ was found to be the most favorable angle for percolation. This result seems to disagree with ISEE magnetic field measurements [*Berchem and Russell*, 1984] indicating that the southward polarity of the interplanetary magnetic field is the most favorable for the formation of FTEs. Other statistical studies (see, for example, *Southwood et al.* [1986]) also show that the occurrence of FTEs is strongly correlated with a southward interplanetary magnetic field.

The conditions of spontaneous excitation of long wave perturbations (wavelength $\lambda_k = 2\pi/k$ much greater than the thickness of the layer L) depend not only on the local values of the plasma parameters near a given magnetic surface within the MCL but also on the initial equilibrium structure of the layer which determines the free energy of the perturbations. It is reasonable to assume that the value $\theta_0 = 60°$ is associated with the symmetrical Harris magnetic field profile and the "constant beta" assumption

$$\frac{8\pi n_{max}(T_e+T_i)}{B_{max}^2} = \frac{8\pi n_0(T_e+T_i)}{B_0^2+B_y^2} = \text{const}$$

which does not result from a self-consistent treatment. For more realistic asymmetrical magnetic field profiles the "preferable" angle could be different and may be sensitive to the degree of asymmetry. The presence of an equilibrium electric field normal to the MCL also may modify the dependence of the marginal thickness on θ_0.

This circumstance significantly complicates the theoretical study of the global stability of the MCL and emphasizes the importance of a proper choice for the initial configuration where some elements of the global pattern are self-consistently included. In other words, to understand how the magnetosheath parameters control the stability of the MCL, factors of asymmetry should be introduced in the equilibrium model (the latter factors emphasize the differences between magnetosheath parameters just outside the MCL and those in the

magnetosphere). These asymmetry factors should control the magnetic and electric fields profiles within the MCL and should finally appear as parameters in the formulation of the stability thresholds.

The effect of the relative flow velocity on collisionless tearing modes in the MCL have been studied by several authors (see, for example, *Lakhina and Schindler* [1983], *Wang and Ashour-Abdalla* [1992], *Kuznetsova et al.* [1994, and references therein]). A temperature gradient has also been taken into account by *Drake et al.* [1983] using fluid equations.

An asymmetrical magnetic field profile was assumed by *Ding et al.* [1992a] in their study of the beta dependence of the collisionless tearing mode growth rate at the dayside magnetopause. In that study, the plasma density distribution corresponding to the given magnetic field profile was determined to satisfy the pressure balance condition, and the power of the free energy source available from the current filamentation (controlling the "strength" of the instability growth) was derived using the expression obtained by *Furth et al.* [1963] in the hydromagnetic approximation. In the study by *Ding et al.* [1992a] the important role of the magnetic field profile across the MCL was emphasized, but the problem of determining the velocity distribution functions corresponding to the chosen magnetic configuration was not discussed.

A considerable amount of effort was made after the pioneering work of *Sestero* [1964, 1966] to construct equilibrium Vlasov models of realistic tangential discontinuities with asymmetrical boundary conditions and large magnetic shears (see, for example, *Alpers* [1969], *Kan* [1972], *Lemaire and Burlaga* [1976], *Roth* [1978, 1979, 1984], *Lee and Kan* [1979], and references cited in these works). However none of these models were used for the stability analysis of the MCL using the Vlasov formalism.

In the present study we investigate the stability of magnetic surfaces with respect to spontaneous excitation of collisionless tearing perturbations within MCLs with asymmetrical magnetic field profiles. The unperturbed MCL is modeled by a "tractable" version (that is, with a minimum number of free parameters) of Vlasov equilibriums used by *Roth* [1978, 1979, 1984] and *Lee and Kan* [1979]. Such an approach enables us to take an electric field normal to the MCL into account, to obtain a more accurate expression for the "free energy" of tearing perturbations, and to consider the finite ion Larmor radius effects and the stabilizing influence of the field-aligned ion oscillations. On the basis of this study the GKZ model is reconsidered and generalized.

Section 2 is devoted to a discussion of several series of Vlasov equilibrium configurations with different asymmetry factors, but with a fixed angle of the magnetic field rotation. In section 3 generalized expressions for the particle adiabatic response to collisionless tearing perturbations are derived and the free energy of these perturbations is calculated. In section 4 the eigenmode set of equations for tearing perturbations in current layers with asymmetrical magnetic field profiles is presented. The criterion of stability for an arbitrary magnetic surface is obtained in section 5. The minimum spatial scale of reconnection patches and the marginal magnetopause thickness for different asymmetry factors are calculated in section 6. The paper ends in section 7 with a summary and the conclusions.

2 Sets of initial configurations

In this paper we consider the magnetopause current layer (MCL) as a one-dimensional slab tangential discontinuity (TD) which is not necessarily charge neutral and which separates two plasmas with different number densities N_1 and N_2, and different magnetic fields $\mathbf{B}_1$ and $\mathbf{B}_2$. The TD is assumed to be parallel to the Y-Z plane and all plasma and field variables only depend on the X coordinate normal to the layer, with a characteristic gradient scale length D. In this configuration the magnetic field $\mathbf{B}$ rotates in the (Y-Z) plane (the total angle of rotation being θ_0; $\theta_0 < 180°$) from $\mathbf{B}_1(0, B_{1y}, B_{1z}) = \mathbf{B}(X \to -\infty)$ in the magnetosheath to $\mathbf{B}_2(0, B_{2y}, B_{2z}) = \mathbf{B}(X \to +\infty)$ in the magnetosphere, while the electric field $\mathbf{E}$ is parallel to the X axis. We also choose the coordinate system in such a way that B_z is equal to zero in the center of the MCL ($X = 0$), but has opposite signs on its outer edges ($B_z < 0$ for $X < 0$, $B_z > 0$ for $X > 0$), while B_y remains everywhere positive. In this configuration, the total angle of the magnetic field rotation θ_0 is then given by

$$\theta_0 = \mathrm{arctg}\,(|B_{1z}|/B_{1y}) + \mathrm{arctg}\,(|B_{2z}|/B_{2y})$$

We consider that the MCL is a mixture of five plasma components, each of them being denoted by a subscript ν, that is, the MCL contains magnetosheath ($\nu = 1$) and magnetospheric ($\nu = 2$) ions, trapped ions ($\nu = 3$) and electrons ($\nu = 4$), and isotropic electrons ($\nu = 5$).

In a TD configuration, a single plasma particle is characterized by three constants of motion: the Hamiltonian (H_ν), and the Y and Z components of the canonical momentum ($P_{\nu y}$ and $P_{\nu z}$)

$$H_\nu = \frac{1}{m_\nu}\left(\mathbf{P}_\nu - \frac{e_\nu}{c}\mathbf{a}\right)^2 + e_\nu\phi = m_\nu v^2/2 + e_\nu\phi$$

$$P_{\nu y} = m_\nu v_y + \frac{e_\nu}{c}a_y, \qquad P_{\nu z} = m_\nu v_z + \frac{e_\nu}{c}a_z$$

In these equations c is the velocity of light in vacuum, e_ν is the charge of the particle of mass m_ν, and $\mathbf{v}(v_x, v_y, v_z)$ its velocity vector, while $\phi(X)$ is the electric potential, and (a_y, a_z) are the Y and Z components of the vector potential. The electric and magnetic field distributions are the derivatives of these potentials

$$E = -d\phi(X)/dX \tag{4}$$

$$B_y = -da_z(X)/dX, \quad B_z = da_y(X)/dX \tag{5}$$

We further assume that the plasma contains only one kind of ions (protons) with an electric charge e, mass m_i and thermal energy T_i ($e_\nu = e$, $m_\nu = m_i$, $T_\nu = T_i$; for $\nu = 1, 2, 3$). Electron components have electric charge $-e$, mass m_e and thermal energy T_e ($e_\nu = -e$, $m_\nu = m_e$, $T_\nu = T_e$; for $\nu = 4, 5$).

The velocity distribution function of ions (F_i) and electrons (F_e) are sums of partial distributions

$$F_i = \sum_{\nu=1}^{3} F_\nu(H_\nu, P_{\nu y}, P_{\nu z}), \tag{6}$$

$$F_e = \sum_{\nu=4}^{5} F_\nu(H_\nu, P_{\nu y}, P_{\nu z})$$

The simplest (and the most generally used way) to solve the Vlasov equation is to use single-valued velocity distribution functions in the (H,P_y,P_z) space. Partial distribution functions are chosen in the following way:

$$F_\nu = s_\nu \left(\frac{m_\nu}{2\pi T_\nu}\right)^{3/2} \exp\left(-\frac{H_\nu}{T_\nu}\right) \mathcal{G}_\nu(P_{\nu y}, P_{\nu z}) \tag{7}$$

with

$$\mathcal{G}_\nu = \frac{1}{2}\mathrm{erfc}\left[\frac{(-1)^\nu c P_{\nu z}}{eB_1\sqrt{D_\nu^2 - \rho_\nu^2}}\right], \quad \nu = 1,2 \tag{8a}$$

$$\mathcal{G}_\nu = C_\nu \exp\left[\frac{(-1)^\nu c P_{\nu y}}{eB_1 D_\nu}\right], \quad \nu = 3,4 \tag{8b}$$

$$\mathcal{G}_\nu = 1, \quad \nu = 5 \tag{8c}$$

where $\mathrm{erfc}(\xi)$ is the complementary error function, $C_\nu = \exp(-\rho_\nu^2/4D_\nu^2)$, and $\rho_\nu = c(2T_\nu m_\nu)^{1/2}/eB_1$ is the particle Larmor radius of the ν species in the asymptotic magnetic field B_1 ($\rho_\nu = \rho_i$ for $\nu = 1,2,3$; $\rho_\nu = \rho_e$ for $\nu = 4,5$). Parameters D_ν are gradient scale lengths which control the number density profiles of each plasma component ν. Collectively, these parameters D_ν determine the magnetopause thickness (see also *Lee and Kan* [1979]) and must be larger than ρ_ν.

When D_ν shrinks to ρ_ν, the complementary error functions in (8) tend to the step functions introduced by *Sestero* [1964]. In what follows we will assume that all spatial gradient scale lengths are the same for all species, that is,

$$D_\nu = D \quad \nu = 1,2,3,4$$

The magnetosheath ion velocity distribution function F_1 approaches a Maxwellian at $X = -\infty$ but tends to zero at $X = +\infty$. Similarly, the magnetospheric ion velocity distribution function F_2 approaches a Maxwellian at $X = +\infty$ but tends to zero at $X = -\infty$ (see equation (8)). These magnetosheath ($\nu = 1$) and magnetospheric ($\nu = 2$) ions are carrying current (J_z) along the Z axis ($J_z = j_{1z} + j_{2z}$, where j_ν are partial current densities) and are responsible for the gradient of B_y. The larger the asymmetry factor

$$\kappa_B = (B_2 - B_1)/B_2 \tag{9}$$

the stronger the J_z current. When $F_1 + F_2$ reduces to an uniform background Maxwellian distribution, the J_z current cancels and B_y remains constant inside the MCL. In this case the asymmetry factor κ_B is equal to zero.

Partial distribution functions F_3 and F_4 correspond to the trapped ions ($\nu = 3$) and electrons ($\nu = 4$) confined within the MCL ($F_{3,4}(X \to \pm\infty) \to 0$). They can also be represented in the form of Maxwellian functions shifted by the diamagnetic drift velocity $u_\nu = cT_\nu/e_\nu B_1 D_\nu$, that is (for $\nu = 3,4$)

$$F_\nu = n_\nu(X) \exp\{-m_\nu[v_x^2 + (v_y - u_\nu)^2 + v_z^2]/2T_\nu\}$$

These particles are carrying current (J_y) along the Y axis ($J_y = j_{3y} + j_{4y}$). The J_y current supports the reversal of B_z. For fixed values of the asymmetry factor κ_B the larger the angle θ_0 the stronger the J_y current. The exponential expression used in (9a) allows us to retrieve the symmetrical charge neutral (ϕ =const) Harris configuration with an analytical solution for a_y when $\kappa_B = 0$

$$a_y = 2DB_1 \ln \cosh(X|B_{1z}|/2DB_1)$$

Although the distribution of trapped particles can be represented by other functions than that used by *Harris* [1962] [see *Roth*, 1979, 1984] we have chosen the particular Harris-type formulation given in (9a) because it gives us an opportunity to compare the results of our stability analysis with previous analytical ones obtained by *Galeev et al.* [1986].

The colder electrons ($T_e \ll T_i$) of magnetosheath and magnetospheric origin denoted by the subscript $\nu = 5$ have a Maxwellian distribution and maintain the global charge neutrality. They carry zero electric current, and their number density variation is mostly determined by the electric potential gradient.

From the velocity distribution functions given in (8)-(9b), partial number densities (n_ν) and current components ($j_{\nu y}$, $j_{\nu z}$) can be calculated as functions of (ϕ, a_y, a_z)

$$n_\nu = s_\nu \exp(-e_\nu \phi / T_\nu) g_\nu(a_y, a_z) \tag{10}$$

$$j_{\nu y} = cT_\nu \partial n_\nu / \partial a_y, \quad j_{\nu z} = cT_\nu \partial n_\nu / \partial a_z \tag{11}$$

where

$$g_\nu = 0.5 \operatorname{erfc}\left[(-1)^\nu a_z / B_1 D_\nu\right], \quad \nu = 1, 2$$

$$g_\nu = \exp\left(-a_y / B_1 D_\nu\right), \quad \nu = 3, 4$$

$$g_\nu = 1, \quad \nu = 5$$

The total ion and electron number densities $n_i(a_y, a_z, \phi)$, $n_e(a_y, a_z, \phi)$ must satisfy the quasi-neutrality condition

$$n(X) = n_i = \sum_{\nu=1}^{3} n_\nu = \sum_{\nu=4}^{5} n_\nu = n_e \tag{12}$$

The ion and electron distribution functions (6) describe a MCL with an asymmetrical magnetic field profile: $B_1 \neq B_2$. In this study we will neglect other possible asymmetries in order to single out the effect of the asymmetry of the magnetic field on the stability properties of the MCL. This simplified model is a tractable version of *Lee and Kan* [1979] and *Roth* [1978, 1979] models. When $B_1 \to B_2$ ($\kappa_B \to 0$) the electric potential (ϕ) is constant inside the transition and $n_5 = n_1 + n_2 = n_b$ = constant. In this limit, the distribution functions (6) tend to the Harris configuration with an uniform background (see equations (1)-(2)). The parameter D is related to the L parameter of the Harris configuration in the following way:

$$L = \frac{2D}{\sin(\theta_0/2)} \tag{13}$$

In our simplified model the structure of the MCL is only determined by the angle of the magnetic field rotation θ_0 and by the factor of asymmetry κ_B. The rotation of the magnetic field vector is controlled by trapped particles ($\nu = 3, 4$), while the increase of its absolute value is supported by the other species ($\nu = 1, 2, 5$).

It is reasonable to assume that the magnetospheric plasma is rather rarefied and to choose $N_2 = n(X \to \infty) = 0.1$ cm^{-3}. For given values of B_1 and B_2 the asymptotic number density on the magnetosheath side $N_1 = n(X \to -\infty)$ is determined from the pressure balance condition

$$8\pi N_1(T_e + T_i) + B_1^2 = 8\pi N_2(T_e + T_i) + B_2^2 \tag{14}$$

Assuming that $\phi_1 = \phi(X \to -\infty) = 0$ and taking account of (10) and of the quasi-neutrality condition (12), it can be seen that

$$s_1 = s_5 = N_1, \quad s_2 = N_2 \left(\frac{N_2}{N_1}\right)^{T_e/T_i} \tag{15}$$

$$\psi_2 = \phi(X = +\infty) = \frac{T_e}{e} \ln \frac{N_2}{N_1} \tag{16}$$

The structure of the MCL is given by the solutions of a set of two second-order differential equations for $a_y(X)$ and $a_z(X)$

$$\frac{d^2 a_y}{dX^2} = -\frac{4\pi}{c} \sum_{\nu=3}^{4} j_{\nu y}(a_y, a_z, \phi) = -\frac{4\pi}{c} J_y \tag{17a}$$

$$\frac{d^2 a_z}{dX^2} = -\frac{4\pi}{c} \sum_{\nu=1}^{2} j_{\nu z}(a_y, a_z, \phi) = -\frac{4\pi}{c} J_z \tag{17b}$$

coupled with the quasi-neutrality equation (12). The differential equations (17), (18a), and (5) form a system of four differential equations of the first order for a_y, a_z, $a_y' = B_z$ and $a_z' = -B_y$. This system is solved numerically using a Hamming's predictor-corrector scheme [*Ralston and Wilf*, 1965]. It is coupled with (12) whose solution is obtained by the Newton-Raphson method for finding the root of a nonlinear algebraic equation [*Press et al.*, 1986]. Starting from the central surface $X = 0$, the system is integrated towards the magnetosheath ($X \to -\infty$) up to the turning point X^*, where both components of the current density become negligibly small, and then back to the magnetosphere ($X \to +\infty$). For the starting values we choose

$$a_y(0) = a_z(0) = 0,$$

$$a_y'(0) = B_z(0) = 0, \quad a_z'(0) = -B_y(0)$$

The values of $B_y(0)$ and $\phi(0)$ can be obtained from the pressure balance condition (14) and from the quasi-neutrality equation (12)

$$B_y(0) = \sqrt{B_1^2 + 8\pi[N_1 - n(0)](T_e + T_i)},$$

$$n(0) = (s_4 + s_5)^{\eta_e} \left[s_3 + 0.5(s_1 + s_2)\right]^{\eta_i},$$

$$\phi(0) = \frac{T_e \eta_i}{e} \ln \frac{s_3 + 0.5(s_1 + s_2)}{s_4 + s_5}.$$

where $\eta_e = T_e/(T_e + T_i)$ and $\eta_i = T_i/(T_e + T_i)$. Parameters s_1, s_2 and s_5 determined from boundary conditions are given in (15). The value of the input parameter $s = s_3 = s_4$ controlling the angle of the magnetic field rotation θ_0 is determined in the following way: for fixed values of B_1 and B_2, an iterative method is used to find the value of s corresponding to a given θ_0. Table 1 gives some computed values of s for $\theta_0 = 120°$, $90°$ and $60°$, and for different values of B_1 and B_2. In this table the asymmetry factor κ_B is also estimated, and it is assumed that $T_i = 4T_e$=1 keV and $D = 2\rho$, where

$$\rho = \frac{c\sqrt{2T_i m_i}}{eB^*} \tag{18}$$

is the typical ion Larmor radius (T_i = 1 keV , B^* =40 nT, ρ = 114.3 km) which will be used as our normalization factor for spatial scales. Note that the values given in Table 1 as well as plasma and field profiles that will be later illustrated practically do not depend on the ratio D/ρ.

Table 1: *computed values of* $s(B_1, B_2, \theta_0)$.

Magnetic field [nT]		Asym. factor	$s = s_3 = s_4$ [cm^{-3}]		
B_1	B_2	κ_B	$\theta_0 = 120°$	$\theta_0 = 90°$	$\theta_0 = 60°$
40	40	0.000	2.384	1.588	0.795
40	43	0.075	2.524	1.677	0.829
40	45	0.111	2.603	1.730	0.850
40	47	0.149	2.674	1.780	0.871
40	50	0.250	2.769	1.853	0.904
40	60	0.333	2.988	2.068	1.014
40	70	0.426	3.104	2.240	1.113
40	80	0.500	3.157	2.380	1.201
50	80	0.375	4.753	3.340	1.641
60	80	0.250	6.415	4.324	2.099
67	80	0.163	7.552	5.021	2.441
70	80	0.125	8.026	5.324	2.596
73	80	0.086	8.492	5.630	2.760
75	80	0.063	8.798	5.838	2.875
80	80	0.000	9.536	6.358	3.179

The electric field $E(X)$ can be either calculated from (4) by numerical differentiation of the electrostatic potential profile $\phi(X)$, or expressed algebraically through a_y, a_z, ϕ, B_y, B_z. The latter expression can be obtained from the quasi-neutrality condition (12)

and expressions for $n_\nu(a_y, a_z, \phi)$, $j_{\nu y}(a_y, a_z, \phi)$, and $j_{\nu z}(a_y, a_z, \phi)$ given in (10) and (11)

$$E = \frac{T_e T_i}{(T_e + T_i) e^2 n(X) c} \left(B_z \frac{\partial J_y}{\partial \phi} - B_y \frac{\partial J_z}{\partial \phi} \right) \tag{19}$$

We will now illustrate how the MCL structure is changing when the factor of asymmetry κ_B is increased, while keeping the angle θ_0 approximately constant. We will consider two groups of MCLs (1 and 2). First, we assume that the magnetic field magnitude on the magnetosheath side is fixed, B_1 =40 nT (case 1), and introduce an asymmetry by increasing the magnetic field B_2 on the magnetospheric side from 40 to 80 nT. This case describes the situation when the increase of the kinetic pressure in the magnetosheath causes an earthward displacement of the MCL toward regions with a larger magnetic pressure. Magnetic field hodograms and number density profiles for fixed B_1 =40 nT and different values of B_2 and θ_0 are shown in the left columns of Figures 1 and 2.

In case 2, we assume that the magnetic field magnitude on the magnetospheric side is fixed, B_2 =80 nT. In this case, the total pressure and the position of the MCL are fixed (because the number density in the magnetospheric adjacent region is a given small parameter N_2 =0.1 cm^{-3}). The increase of the kinetic pressure in the adjacent magnetosheath region results in a corresponding reduction of the magnetic pressure. This will introduce an asymmetry in the magnetic field profile, that is, a decrease of the magnetic field B_1 on the magnetosheath side from 80 to 40 nT. Magnetic field hodograms and number density profiles for B_2 =80 nT are shown in the right columns of Figures 1 and 2, for different values of B_1 and θ_0.

The number density profiles in Figure 2 are illustrated as a function of the distance X/ρ from the center of the layer $X = 0$. It is seen that the introduction of asymmetry in case 1 (the left column) significantly modifies the number density in the center of the layer, while in case 2 (the right column) the number densities at $X = 0$ are only slightly different for various asymmetry factors.

Plasma and field parameters characterizing the structure of the MCL are illustrated in Figure 3 for $\theta_0 = 120°$, B_1 =40 nT, and for different values of B_2. It can be seen that when θ_0 is fixed, the profiles of B_z and J_y only slightly differ from those obtained from the symmetrical ($B_2 = B_1$) Harris case, while B_y and J_z are significantly modified with the increase of the asymmetry (that is, the increase of B_2). This means that the asymmetry is mainly controlled by the J_z current. The profiles for $\phi(X)$ and $E(X)$ show that even a small asymmetry (for example, $\kappa_B = 0.25$) results in a significant drop of the potential across the layer $\Delta\phi \sim 700$ V (with a maximum value of the electric field of the order of 0.5 mV/m near $X = 0$).

In the following sections we will study the stability of the equilibrium configurations illustrated in Figures 1–3. The first necessary step in establishing the threshold conditions for global magnetic reconnection is to study the instability at a given magnetic surface within the MCL.

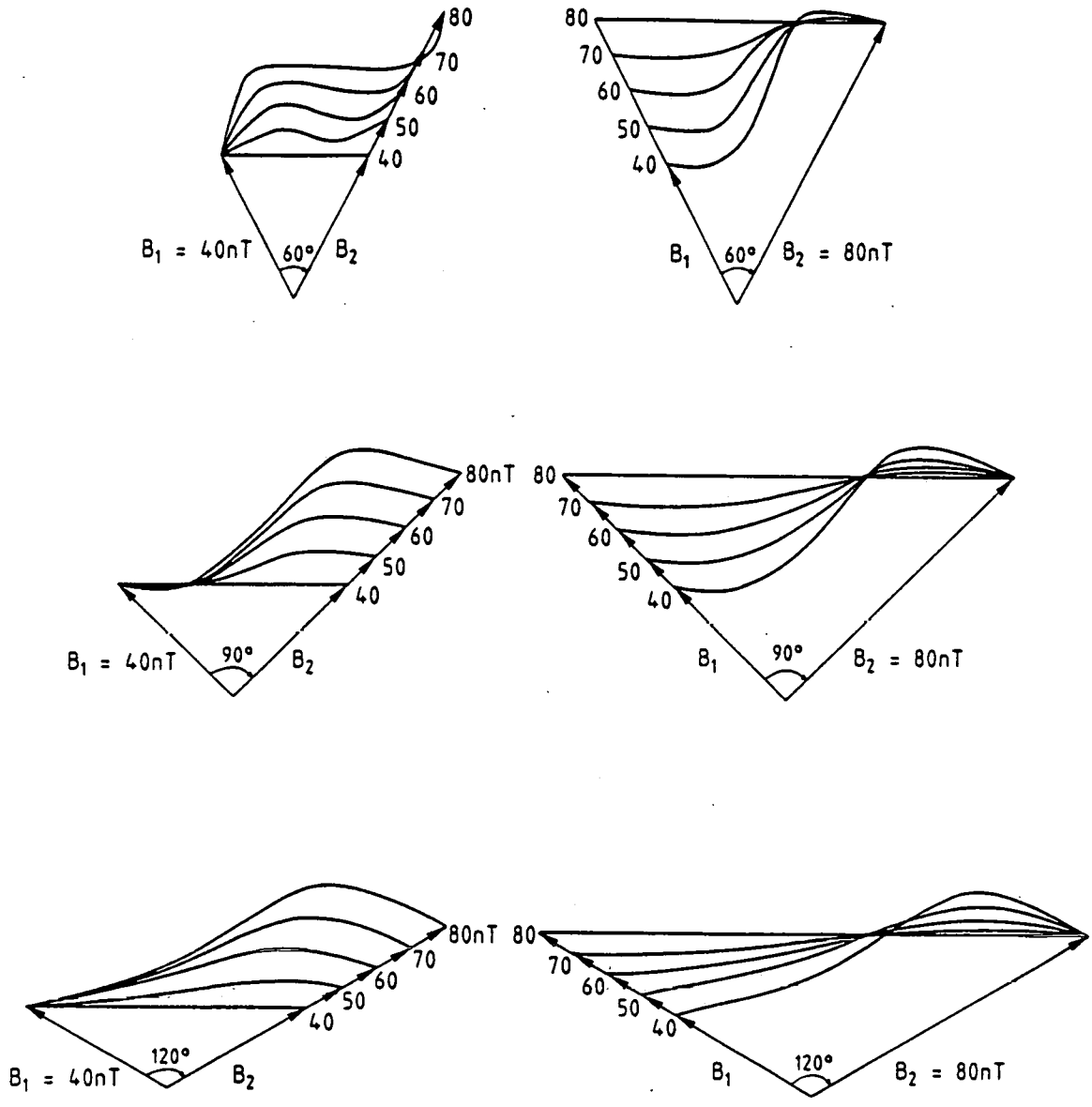

Figure 1: Hodograms of **B** (in nanoteslas) through the magnetopause current layer for different values of B_1, B_2, and θ_0. (left) Case 1: The magnitude of the magnetic field in the adjacent magnetosheath region is fixed, B_1=40 nT, while the intensity of the magnetospheric field (B_2) is changing from 40 to 80 nT. (right) Case 2: The magnitude of the magnetic field in the adjacent magnetospheric region is fixed, B_2=80 nT, while the intensity of the magnetic field in the adjacent magnetosheath (B_1) is changing from 80 to 40 nT. From top to bottom the angle of the magnetic field rotation θ_0 is changing from 60° to 120°. These MCL hodograms have been calculated with the following parameter values: $N_2 = 0.1$ cm^{-3}, $T_i = 4T_e = 1$ keV, $D = 2\rho$ (ρ is the Larmor radius of a ion with a typical thermal energy of 1 keV, in a magnetic field intensity of 40 nT, $\rho = 114.3$ km). The value of the parameter $s = s_3 = s_4$ depends on the values of θ_0, B_1, and B_2 as computed in Table 1.

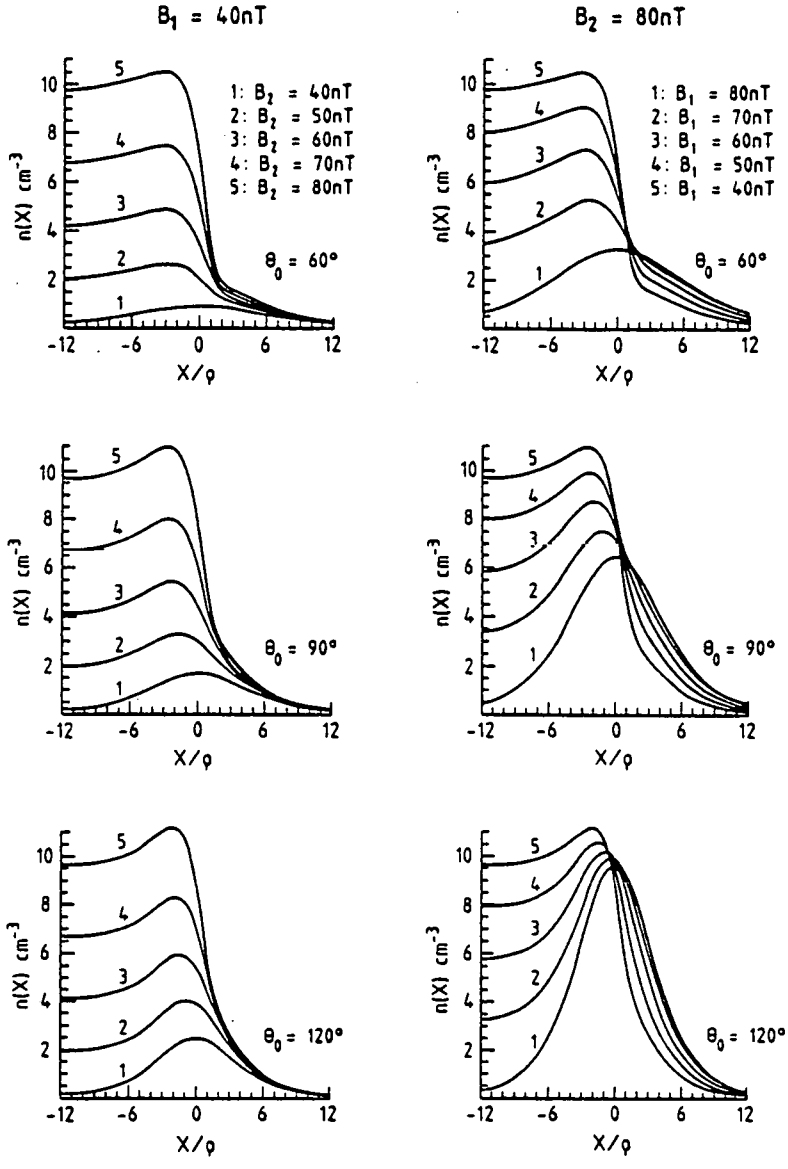

Figure 2: Number density profiles $n(X)$ (per cubic centimeters) corresponding to the magnetic field hodograms shown in Figure 1 as a function of the normalized distance X/ρ from the center of the layer ($X = 0$).

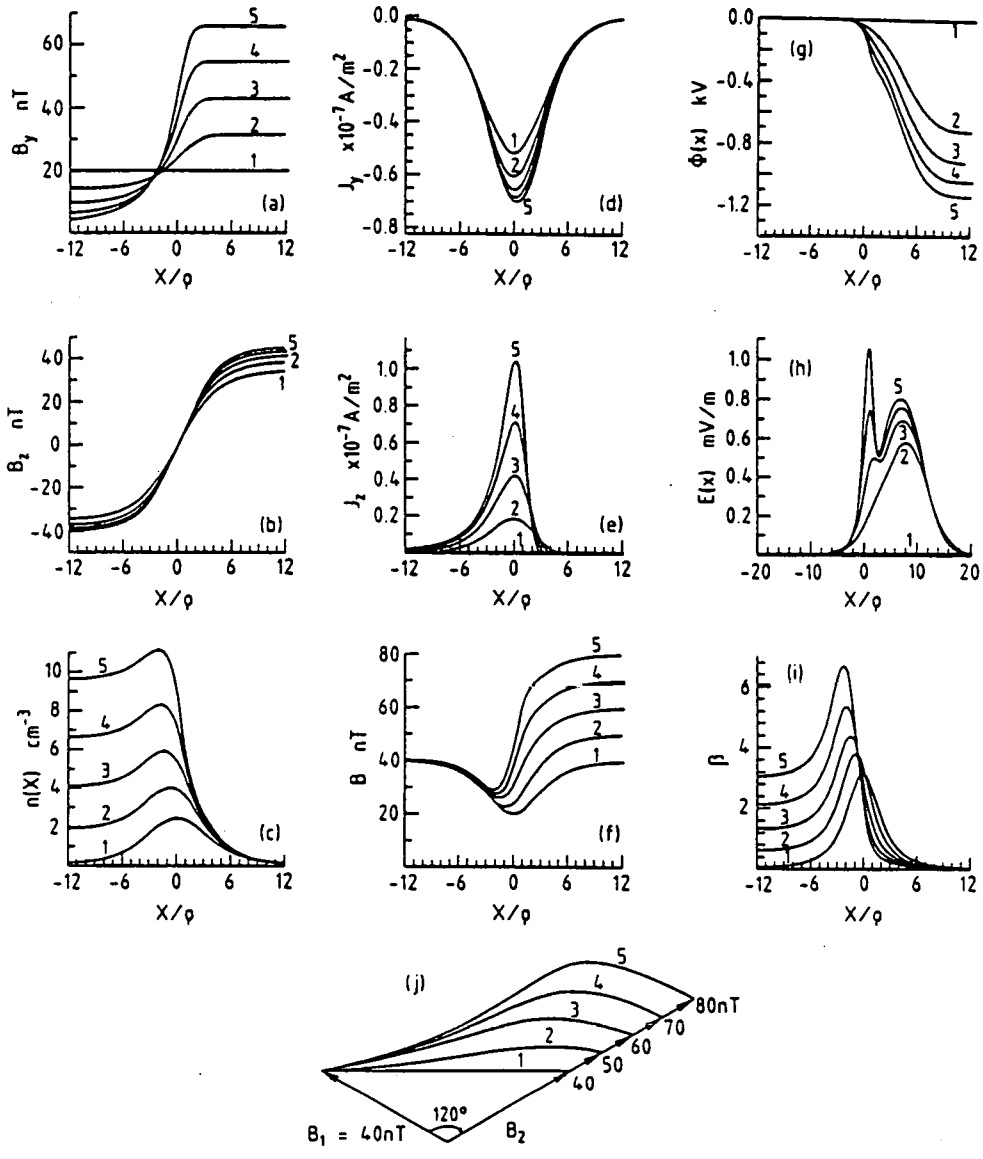

Figure 3: Structure of the magnetopause current layer for $\theta_0 = 120°$, $N_2 = 0.1$ cm^{-3}, $T_i = 4T_e = 1$ keV, $B_1 = 40$ nT, and different values of B_2 (1, $B_2 = 40$ nT; 2, $B_2 = 50$ nT; 3, $B_2 = 60$ nT; 4, $B_2 = 70$ nT; 5, $B_2 = 80$ nT). Plasma and field parameters are illustrated as a function of the distance X/ρ from the center of the layer ($X = 0$) (ρ is the Larmor radius of a ion with a typical thermal energy of 1 keV, in a magnetic field intensity of 40 nT, $\rho = 114.3$ km). It is also assumed that $D = 2\rho$. The symmetrical Harris profiles correspond to curves 1 ($B_2 = 40$ nT). From top to bottom and from left to right, the following variables are illustrated: (a) B_y (in nanoteslas); (b) B_z (in nanoteslas); (c) number density $n(X)$ (per cubic centimeters); (d) $J_y = j_{3y} + j_{4y}$ (10^{-7} A/m^2); (e) $J_z = j_{1z} + j_{2z}$ (10^{-7} A/m^2); (f) magnitude of the magnetic field B (in nanoteslas); (g) electric potential $\phi(X)$ (in kilovolts); (h) electric field $E(X)$ (in millivolts per meter); (i) plasma beta ($\beta(X) = 8\pi n(X)(T_i + T_e)/B^2(X)$); (j) the hodograms of $\mathbf{B}$ (in nanoteslas).

3 Adiabatic response to tearing perturbations in the outer region

Let us consider the stability of an arbitrary magnetic surface $X = X_S$ of the plasma configuration modeled in the previous section with respect to the excitation of low-frequency tearing-type electromagnetic perturbations. Such perturbations can be described by small variations $\tilde{A}_y$, $\tilde{A}_z$, and $\tilde{\varphi}$ superposed on the equilibrium vector and scalar potentials a_y, a_z, and ϕ

$$A_y = a_y + \tilde{A}_y, \quad A_z = a_z + \tilde{A}_z, \quad \varphi = \phi + \tilde{\varphi}, \tag{20}$$

These perturbations depend on both the Y and Z coordinates and on the time t in the form of a plain wave

$$\tilde{A}_y, \tilde{A}_z, \tilde{\varphi} \sim \exp(-\imath\omega t + \imath k_z z + \imath k_y y) \tag{21}$$

where ω $(= \omega_r + \imath\gamma)$ is the complex frequency and $\mathbf{k}(0, k_y, k_z)$ is the wave vector perpendicular to the local direction of the equilibrium magnetic field at $X = X_S$

$$k_\perp(X_S) = k, \qquad k_\parallel(X_S) = 0 \tag{22}$$

Subscripts "$\parallel$" and "$\perp$" refer to the vector components parallel and perpendicular to the local direction of the magnetic field $\mathbf{B}(X)$. For instance,

$$k_\parallel(X) = \frac{k_y B_y + k_z B_z}{B}, \quad k_\perp(X) = \frac{-k_y B_z + k_z B_y}{B}$$

$$A_\parallel(X) = \frac{\tilde{A}_y B_y + \tilde{A}_z B_z}{B}, \quad A_\perp(X) = \frac{-\tilde{A}_y B_z + \tilde{A}_z B_y}{B}$$

For such perturbations the inductive and potential parts of the parallel perturbed electric field $\tilde{E}_\parallel(X)$ cannot compensate each other in some small vicinity of the $X = X_S$ plane. Therefore $\tilde{E}_\parallel$ has a finite value in this region which results in a strong nonadiabatic interaction of electromagnetic perturbations with particles. The plane $X = X_S$ is usually called the singular surface for the $\mathbf{k}$-mode $(\mathbf{k} \cdot \mathbf{B}(X_S) = 0)$. Far from the singular surface, that is, in the "outer region" $\tilde{E}_\parallel(X) \to 0$ and the nonadiabatic contribution to the interaction becomes negligibly small.

In this outer region the reversible adiabatic response of particles to tearing perturbations can be derived immediately from the equilibrium distribution. Let us assume that adiabatic contributions to the perturbed electric current and number density can be expressed as functions of φ, A_y, and A_z. Using the Taylor expansion series for $\tilde{A}_y \ll a_y$, $\tilde{A}_z \ll a_z$, $\tilde{\varphi} \ll \phi$, we obtain the linearized Maxwell equations and the quasi-neutrality condition for perturbations in the outer region in the following form:

$$\frac{d^2\tilde{A}_y}{dX^2} - k^2\tilde{A}_y = -4\pi\left(d_1\tilde{A}_y + d_3\tilde{A}_z - b_1\tilde{\varphi}\right) \tag{23a}$$

$$\frac{d^2\tilde{A}_z}{dX^2} - k^2\tilde{A}_z = -4\pi\left(d_2\tilde{A}_z + d_3\tilde{A}_y - b_2\tilde{\varphi}\right) \tag{23b}$$

$$b_1\tilde{A}_y + b_2\tilde{A}_z + b_0\tilde{\varphi} = 0 \tag{23c}$$

where

$$d_1 = \frac{1}{c}\frac{\partial J_y}{\partial a_y} = \frac{\partial^2 G}{\partial a_y^2} = \frac{1}{B_1^2 D^2}\sum_{\nu=3}^{4} T_\nu n_\nu \tag{24a}$$

$$d_2 = \frac{1}{c}\frac{\partial J_z}{\partial a_z} = \frac{\partial^2 G}{\partial a_z^2} = \frac{2a_z T_i}{B_1^2 D^2}\sum_{\nu=1}^{2}\frac{\partial n_\nu}{\partial a_z} \tag{24b}$$

$$d_3 = \frac{1}{c}\frac{\partial J_y}{\partial a_z} = \frac{1}{c}\frac{\partial J_z}{\partial a_y} = \frac{\partial^2 G}{\partial a_y \partial a_z} = 0 \tag{24c}$$

$$b_0 = \sum_{\nu=1}^{5} e_\nu \frac{\partial n_\nu}{\partial \phi} = -\frac{\partial^2 G}{\partial \phi^2} = -e^2 n(X)\frac{T_e + T_i}{T_e T_i} \tag{24d}$$

$$b_1 = -\frac{\partial^2 G}{\partial a_y \partial \phi} = -\frac{1}{c}\frac{\partial J_y}{\partial \phi} = \frac{e}{B_1 D}\sum_{\nu=3}^{4}(-1)^\nu n_\nu \tag{24e}$$

$$b_2 = -\frac{\partial^2 G}{\partial a_z \partial \phi} = -\frac{1}{c}\frac{\partial J_z}{\partial \phi} = \frac{e}{4\pi T_i}\frac{dB_y}{dX} \tag{24f}$$

$$G(a_y, a_z, \phi) = \sum_{\nu=1}^{5} n_\nu T_\nu \tag{24g}$$

and $J_y(a_y, a_z, \phi)$, $J_z(a_y, a_z, \phi)$, and $n_\nu(a_y, a_z, \phi)$ are the equilibrium current and number densities given in section 2.

Let us introduce the functions $A_1(X)$ and $A_2(X)$

$$A_1 = \tilde{A}_y\frac{k_z}{k} - \tilde{A}_z\frac{k_y}{k} = A_\parallel\frac{k_\perp}{k} - A_\perp\frac{k_\parallel}{k} \tag{25a}$$

$$A_2 = \tilde{A}_y\frac{k_y}{k} + \tilde{A}_z\frac{k_z}{k} = A_\parallel\frac{k_\parallel}{k} + A_\perp\frac{k_\perp}{k} \tag{25b}$$

Since

$$A_1(X = X_S) = A_\parallel, \qquad A_2(X = X_S) = A_\perp$$

we call functions $A_1(X)$ and $A_2(X)$ quasi-parallel and quasi-perpendicular components of the perturbed vector potential $\tilde{\mathbf{A}}(0, \tilde{A}_y, \tilde{A}_z)$. Substituting expressions (25) and (26a) into equations (23) and (24a), and eliminating $\tilde{\varphi}$ by taking into account condition (23c), the set of eigenmode equations in the outer region can be reduced to the following form

$$\frac{d^2 A_1}{dX^2} - k^2 A_1 = V_{11}A_1 + V_{12}A_2 \tag{26a}$$

$$\frac{d^2 A_2}{dX^2} - k^2 A_2 = V_{21}A_1 + V_{22}A_2 \tag{26b}$$

Terms V_{11}, V_{12}, V_{21} and V_{22} depending on the global plasma distribution are proportional to the perturbed current density responsible for the reversible adiabatic interaction of electromagnetic perturbations with particles

$$V_{11} = -4\pi \left[c_1 \cos^2\theta + c_2 \sin^2\theta - c_3 \sin 2\theta\right] \tag{27a}$$

$$V_{12} = V_{21} = -2\pi \left[(c_1 - c_2)\sin 2\theta + 2c_3 \cos 2\theta\right] \tag{27b}$$

$$V_{22} = -4\pi \left[c_1 \sin^2\theta + c_2 \cos^2\theta + c_3 \sin 2\theta\right] \tag{27c}$$

where

$$c_1 = d_1 + \frac{b_1^2}{b_0}, \quad c_2 = d_2 + \frac{b_2^2}{b_0}, \quad c_3 = d_3 + \frac{b_1 b_2}{b_0}$$

and θ is the angle between the wave vector $\mathbf{k}$ and the Z axis

$$\sin\theta = \frac{k_y}{k} = -\frac{B_z(X_z)}{B(X_S)}, \quad \cos\theta = \frac{k_z}{k} = \frac{B_y(X_z)}{B(X_S)}$$

For the symmetrical case b_1=b_2=d_3=0, and equations (26a) and (26b) are not coupled any more at $X_S = 0$ (where $\sin\theta = 0$). For the general asymmetrical case ($\kappa_B \neq 0$) equations for A_1 and A_2 are coupled even for $X_S = 0$. Using the same approximate gauge condition as in the GKZ model, that is

$$k_y \tilde{A}_y + k_z \tilde{A}_z = 0 \tag{28}$$

which means that the coupling between quasi-parallel ("tearing") and quasi-perpendicular ("alfven") modes is neglected (that is, $dA_x/dX \approx 0$, $A_2 \approx 0$), the set of eigenmode equations (26a) and (26b) is reduced to a single equation

$$\frac{d^2 A_1}{dX^2} - k^2 A_1 = V_0 A_1, \quad V_0 = V_{11} \tag{29}$$

The asymmetry of the magnetic field profile ($B_2 \neq B_1 \Rightarrow \kappa_B \neq 0$) modifies the well-known potential well

$$V_0 = B_z''/B_z = -2L^{-2}\cosh^{-2}(X/L)\cos^2\theta$$

corresponding to the symmetrical Harris case ($B_2 = B_1 \Rightarrow \kappa_B = 0$), in the following way:

$$V_0 = \frac{B_y''}{B_y}\sin^2\theta + \frac{B_z''}{B_z}\cos^2\theta + \frac{T_e}{2T_i}\frac{dB_y^2/dX}{B_z^2} \tag{30}$$

$$\times \left(\cos\theta - \frac{B_z}{B_y}\sin\theta\right)^2 \left(\frac{dB_y^2/dX}{8\pi n(X)(T_e + T_i)} - \frac{eE}{T_e}\right)$$

The solution of (29) for a given magnetic surface $X = X_S$

$$A_1(X < X_S) = A_1^-(X), \quad A_1(X > X_S) = A_1^+(X)$$

should satisfy the following boundary conditions:

$$A_1^{\mp}(X \to \mp\infty) \sim e^{\pm kX} \to 0$$

For the symmetrical case (κ_B=0) the solution of (29) can be analytically expressed through associated Legendre's functions

$$\begin{aligned} A_1(X < X_S) &= C^- P_l^{-m}\left(-\tanh\frac{X}{L}\right) \\ A_1(X > X_S) &= C^+ P_l^{m}\left(\tanh\frac{X}{L}\right) \end{aligned}$$

where $l = 0.5(\sqrt{1 + 8\cos^2\theta} - 1)$, $m = kL$.

For the general asymmetrical case ($\kappa_B \neq 0$) the eigenmode equation (29) in the outer region is solved numerically. Introducing the variable $R(X)$ which is the logarithmic derivative of the function A_1 (see the Ricatti transform method used by *Gladd* [1990])

$$R(X) = \frac{dA_1/dX}{A_1}$$

$$R(X < X_S) = R^-(X), \quad R(X > X_S) = R^+(X)$$

equation (29) can be reduced to a nonlinear first-order differential equation

$$\frac{dR}{dX} = k^2 + V_0 - R^2 \tag{31}$$

with the following boundary conditions: $R(X \to \mp\infty) \to \pm k$.

The structure of the outer solution $A_1(X)$ is shown on Figures 4 and 5 for different θ_0, κ_B, X_S, and kD. The dashed curves on each of these figures (curves denoted "1S" for $X_S = -0.4D$, "2S" for $X_S = 0$, and "3S" for $X_S = 0.4D$) correspond to symmetrical Harris profiles, that is, to the case where $\kappa_B = 0$ ($B_2 = B_1$). The solid curves (denoted 1, $X_S = -0.4D$; 2, $X_S = 0$; and 3, $X_S = 0.4D$) correspond to asymmetrical magnetic field profiles with $\kappa_B = 0.5$ ($B_2 = 2B_1$). The normalization is chosen in the following way:

$$A_1^-(X = -6D) = 1$$

$$A_1^-(X = X_S - 0) = A_1^+(X = X_S + 0)$$

The first derivative of the outer solution A_1 is discontinuous at $X = X_S$, that is, $R^-(X \to X_S - 0) \neq R^+(X \to X_S + 0)$. The jump of the solution of (31) (the logarithmic derivative of the outer solution A_1) at $X = X_S$

$$\Delta' = R^+(X \to X_S + 0) - R^-(X \to X_S - 0) \tag{32}$$

is proportional to the power of the free energy source available from current filamentation. This term contains information about the global distribution of plasma and magnetic field in the layer.

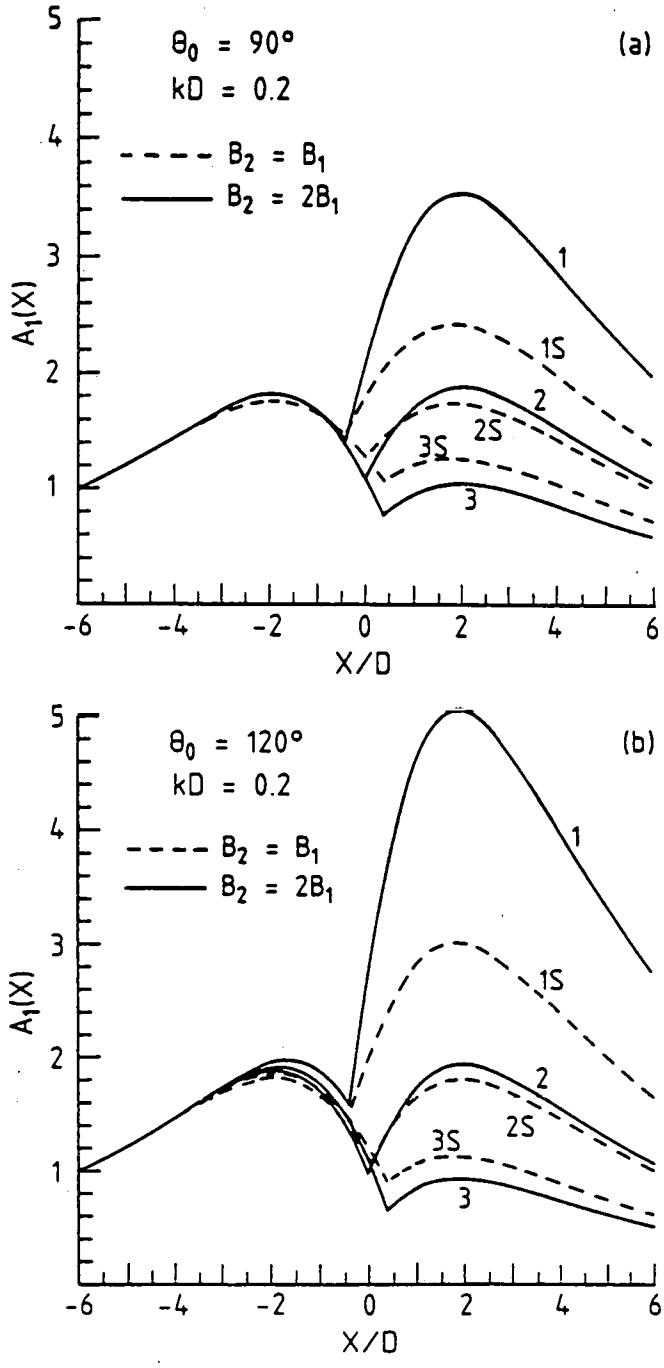

Figure 4: Spatial forms of the outer solution for $kD = 0.2$ and $B_1 = 40$ nT. The angle of the magnetic field rotation is (a) $\theta_0 = 90°$ and (b) $\theta_0 = 120°$. The six curves correspond to different values of κ_B and X_S: (1) $X_S = -0.4D$, $\kappa_B = 0.5$; (1S) $X_S = -0.4D$, $\kappa_B = 0$; (2) $X_S = 0$, $\kappa_B = 0.5$; (2S) $X_S = 0$, $\kappa_B = 0$; (3) $X_S = 0.4D$, $\kappa_B = 0.5$; (3S) $X_S = 0.4D$, $\kappa_B = 0$. The dashed curves (1S), (2S), and (3S) correspond to symmetrical Harris profiles.

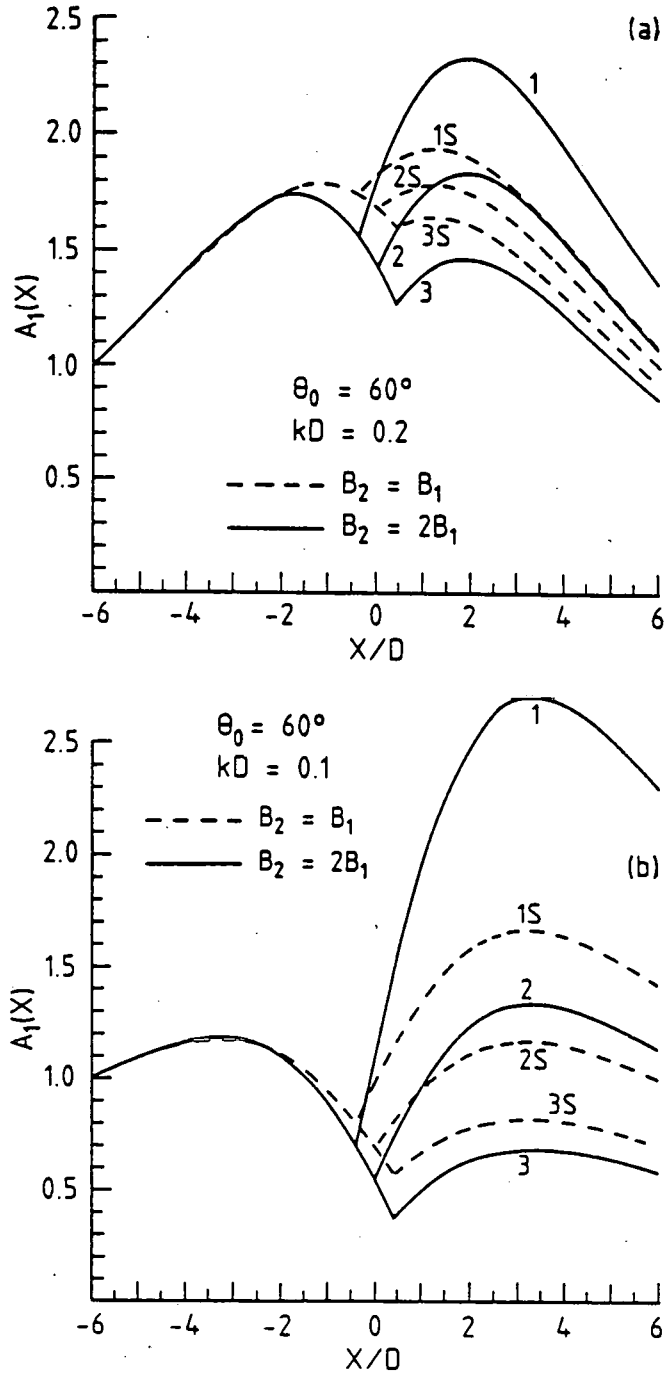

Figure 5: Spatial forms of the outer solution for $\theta_0 = 60°$ and $B_1 = 40$ nT. (a) $kD = 0.2$; (b) $kD = 0.1$. The six curves correspond to different values of κ_B and X_S and are denoted in the same way as in Figure 4. The dashed curves (1S), (2S), and (3S) correspond to symmetrical Harris profiles.

For the symmetrical Harris equilibrium ($B_1 = B_2$) the expression for Δ' can be analytically calculated for arbitrary magnetic surfaces within the layer and expressed through the associated Legendre functions [see *Kuznetsova and Zelenyi*, 1985, p. 367]. For $X_S = 0$ this expression reduces to the well-known form

$$\Delta'(kL) = \Delta'_0 = \frac{1 - (kL)^2}{kL^2}$$

The dependences of the free energy of perturbations Δ' on the wave number kD modified by the finite asymmetry are calculated from (32) and are illustrated in Figure 6 for different θ_0 and X_S. The dashed curves on each of these panels correspond to the symmetrical Harris equilibrium ($\kappa_B = 0$). The dotted curves correspond to asymmetrical magnetic field profiles with $\kappa_B = 1/3$, while the solid curves correspond to the most asymmetrical configurations with $\kappa_B = 1/2$.

When $\Delta'(X_S, kD, \kappa_B, \theta_0) > 0$ the magnetic surface X_S within the MCL with given θ_0, κ_B, and D has an excess of free energy with respect to the excitation of perturbations with wavelengths $2\pi/k$. Figure 6 shows that configurations with the largest degree of asymmetry κ_B have the largest excess of free energy Δ' for the same θ_0, X_S, and kD. Hence the asymmetrical transitional layers are potentially more unstable than the symmetrical ones. Whether this tendency will be realized depends on other contributions to the energy balance condition associated with irreversible nonadiabatic responses of resonant particles to perturbations inside the interaction region $|x| < \delta_\varphi$. This will be calculated in the following section.

4 The set of eigenmode equations

The first-order perturbation of the velocity distribution function

$$\tilde{f}_i = \sum_{\nu=1}^{3} \tilde{f}_\nu, \quad \tilde{f}_e = \sum_{\nu=4}^{5} \tilde{f}_\nu$$

is obtained by integrating the linearized Vlasov equation along the unperturbed particle trajectory

$$\tilde{f}_\nu = \tilde{f}_\nu^{\text{ad}} + \tilde{f}_\nu^{\text{res}} \tag{33}$$

where the first term corresponds to the solutions in the outer region illustrated in previous section

$$\tilde{f}_\nu^{\text{ad}} = \frac{e_\nu}{c}\left(\frac{\partial F_\nu}{\partial P_{\nu y}}\tilde{A}_y + \frac{\partial F_\nu}{\partial P_{\nu z}}\tilde{A}_z + \frac{\partial F_\nu}{\partial H_\nu}c\tilde{\varphi}\right) \tag{34a}$$

This term associated with the reversible change in the distribution depends only on the form of the equilibrium distribution function. The second term in (33) represents the irreversible change in the distribution and depends on the details of the particle orbits

$$\tilde{f}_\nu^{\text{res}} = -\imath\frac{e_\nu}{c}(\hat{D}F_\nu)\int_{-\infty}^{t}(v_\parallel A_\parallel + u_{D\nu}A_\perp - c\tilde{\varphi})\,d\tau \tag{34b}$$

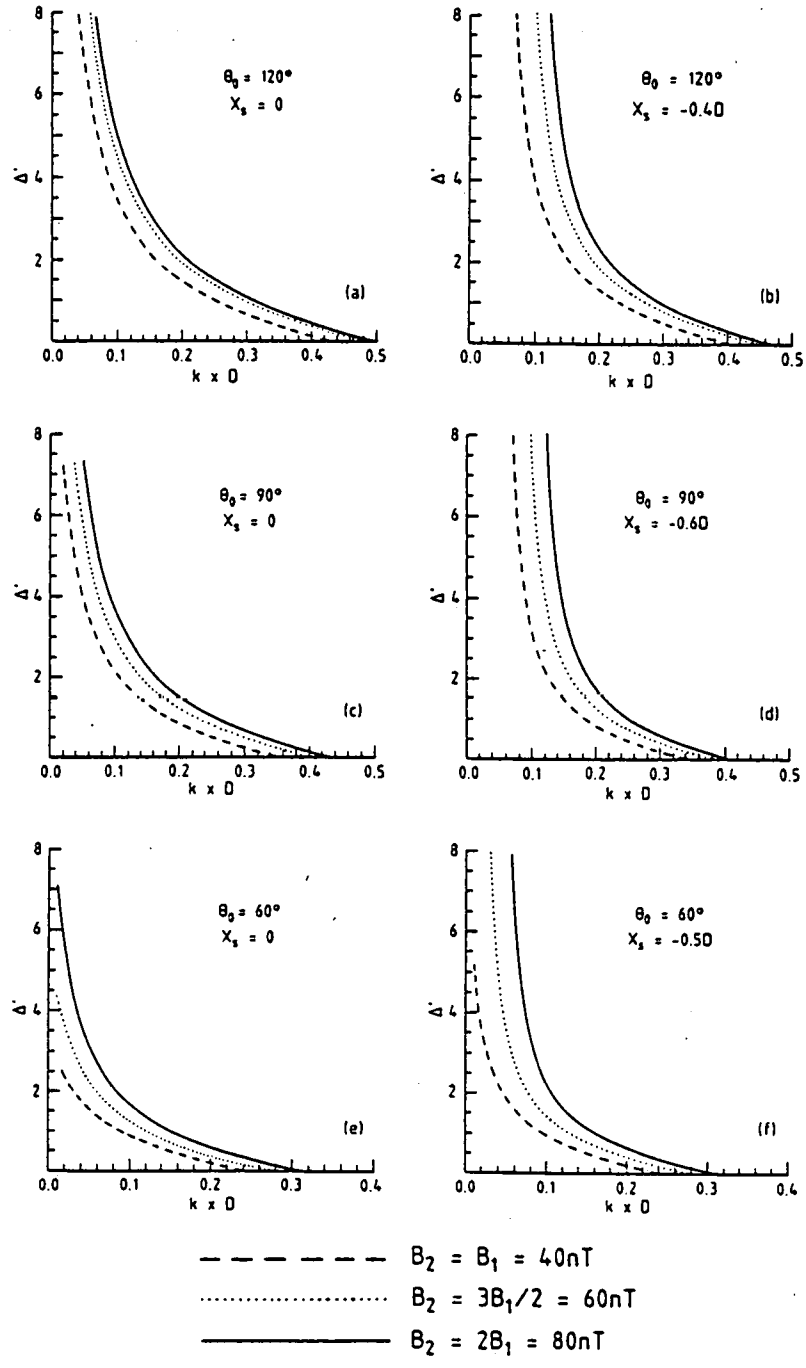

Figure 6: Free energy of the perturbations Δ' as a function of the wave number kD for different values of θ_0, X_S, and κ_B. The dashed curves on each panel correspond to the symmetrical Harris equilibrium ($B_1 = B_2 = 40$ nT; $\kappa_B = 0$). The dotted curves correspond to asymmetrical magnetic field profiles with $\kappa_B = 1/3$, while the solid curves correspond to the most asymmetrical configurations with $\kappa_B = 1/2$.

where

$$(\hat{D}F_\nu) = \left(\omega\frac{\partial F_\nu}{\partial H_\nu} + k_y\frac{\partial F_\nu}{\partial P_{\nu y}} + k_z\frac{\partial F_\nu}{\partial P_{\nu z}}\right)$$

and $u_{D\nu}$=u_E+$u_{B\nu}$ are averaged guiding center drifts perpendicular to the magnetic field ($\mathbf{u}_E$=$c[\mathbf{E}\times\mathbf{B}]/B^2$, $\mathbf{u}_{B\nu}$=$-cT_\nu[\nabla B\times\mathbf{B}]/e_\nu B^3$).

Let us adopt the gauge condition (28) and assume that in the δ_φ vicinity of the singular surface $X = X_S$: $A_\perp \approx A_2 \approx 0$ and $A_\parallel \approx A_1$. An eigenmode equation for the quasi-parallel component A_1 where the nonadiabatic terms are taken into account is obtained by considering the linearized Maxwell equation

$$\frac{d^2A_1}{dX^2} - k^2A_1 - V_0A_1 = \hat{V}A_1 \tag{35}$$

The term $\hat{V}A_1$ corresponds to the singular current due to the nonadiabatic response of the particles near $X = X_S$

$$\hat{V}A_1 = -\frac{4\pi}{c}\sum_{\nu=1}^{5} e_\nu \int (v_y\cos\theta - v_z\sin\theta)\tilde{f}_\nu^{\rm res}\,d\mathbf{v} \tag{36}$$

This equation is coupled with the quasi-neutrality condition

$$b_0\tilde{\varphi} + b_3A_1 = -\sum_{\nu=1}^{5} e_\nu \int \tilde{f}_\nu^{\rm res}\,d\mathbf{v} \tag{37}$$

The singular current which is strongly peaked near the singular surface $X = X_S$ is controlled by the local values of the plasma density and magnetic field in the singular region

$$|x| = |X - X_S| < |\delta_\nu|, \qquad \delta_\nu = \frac{\bar{\omega}_\nu}{k_\parallel' v_{T\nu}}$$

where $\bar{\omega}_\nu = \omega - \omega_E - \omega_{D\nu}$, $\omega_E \approx ku_E(X_S)$, $\omega_{D\nu} \approx ku_{D\nu}(X_S)$, $v_{T\nu} = \sqrt{2T_\nu/m_\nu}$, and

$$k_\parallel' = \frac{dk_\parallel}{dx}(x=0) = \frac{k_zB_z'(X_S) + k_yB_y'(X_S)}{B(X_S)}$$

It can be seen that

$$\delta_1 = \delta_2 = \delta_3 = \delta_i, \quad \delta_4 = \delta_5 = \delta_e$$

Assuming that all particles are magnetized and that their Larmor radius is smaller than the spatial inhomogeneity gradient scale the trajectory integrals in (34b) can be evaluated in the guiding center approximation, and the singular current (36) can be reduced to the following form

$$\hat{V}A_1 = \frac{k_\perp}{k}\left\{\sum_{\nu=1}^{5}\hat{V}_\nu\left(A_1 - \frac{k_\parallel c}{\bar{\omega}_\nu}\hat{\Gamma}_\nu\tilde{\varphi}\right) + \hat{R}_iA_1\right\} \tag{38}$$

Operators $\hat{V}_\nu$, $\hat{\Gamma}_\nu$, and $\hat{R}_i$ are given by

$$\hat{V}_\nu = -\frac{2\omega_{p\nu}^2}{c^2}\zeta_\nu^2 S_{\nu 1} \tag{39a}$$

$$\hat{\Gamma}_\nu = I_0(\frac{1}{2}\rho_{x\nu}^2\hat{k}_x^2)\exp(-\frac{1}{2}\rho_{x\nu}^2\hat{k}_x^2) \tag{39b}$$

$$\hat{R}_i = \beta(X)\eta_i\sum_{\nu=1}^{3}\zeta_\nu S_{\nu 2}\hat{k}_x^2 \tag{39c}$$

where $\hat{k}_x = -\imath(\partial/\partial x)$ is a differential operator, I_0 is the modified Bessel function of order 0, $\rho_{x\nu}$=$\rho_\nu B_1/B(X_S)$ is the particle Larmor radius in the local magnetic field $B(X_S)$, $\omega_{p\nu}$=$[4\pi n(X)e^2/m_\nu]^{1/2}$ is the plasma frequency, and

$$\zeta_\nu = \frac{\bar{\omega}_\nu}{k_\parallel v_{T\nu}} \approx \frac{\delta_\nu}{x}$$

Functions $S_{\nu 1}$ and $S_{\nu 2}$ in (39a) and (39c) come from averaging the perturbed distribution functions over the normalized parallel velocity ($\overline{v}_\parallel = v_\parallel/v_{T\nu}$)

$$S_{\nu(n+1)} = W_{\nu(n+1)} + W_{\nu n}\frac{(b_1B_y + b_2B_z)c}{b_0Bv_{T\nu}}$$

$$W_{\nu n} = -\frac{T_\nu}{n(X)\bar{\omega}_\nu}\int(\hat{D}F_\nu)\frac{\overline{v}_\parallel{}^n\,d\mathbf{v}}{\overline{v}_\parallel - \zeta_\nu}$$

Index n can take any integer values: $n = 0, 1, 2, \ldots$. Neglecting terms proportional to $\rho_{x\nu}/D$ functions $W_{\nu n}$ can be approximately expressed through the plasma dispersion function (Z_n)

$$W_{\nu n} \approx \left[\frac{n_\nu}{n(X)} - \frac{\omega_\nu^*}{\bar{\omega}_\nu}\right]Z_n(\zeta_\nu) \tag{40}$$

$$Z_n(\zeta) = \frac{1}{\sqrt{\pi}}\int_{-\infty}^{\infty}\frac{t^n\exp(-t^2)\,dt}{t - \zeta - i\epsilon\mathrm{sign}\zeta}, \quad \epsilon \to 0$$

In (40), ω_ν^* is the local drift frequency of the ν species

$$\omega_\nu^* = -\frac{c\mathbf{k}[T_\nu\nabla n_\nu \times \mathbf{B}]}{e_\nu B^2 n(X)}$$

$$= \left[-\omega_E\frac{n_\nu}{n(X)} + \frac{cT_\nu k}{e_\nu n(X)}\left(\sin\theta\frac{\partial n_\nu}{\partial a_y} + \cos\theta\frac{\partial n_\nu}{\partial a_z}\right)\right]_{X=X_S}$$

The ion (ω_i^*) and electron (ω_e^*) drift frequencies are then

$$\omega_i^* = \sum_{\nu=1}^{3}\omega_\nu^*, \quad \omega_e^* = \sum_{\nu=4}^{5}\omega_\nu^*$$

Operator $\hat{V}_\nu$ (see equation (39a)) comes from integrating along the particle motion parallel to the magnetic field lines. The nonlinear operators $\hat{\Gamma}_\nu$ (see equation (39b)) and $\hat{R}_i$ (see equation (39c)) come from averaging over the particle motion along the Larmor orbit.

The term proportional to $\hat{R}_i$ describes slow variations of A_1 across the layer (perpendicular to the magnetic field) and corresponds to corrections associated with deviations from the "A_1 = const" approximation. For electrons ($\nu = 4, 5$) $\Gamma_\nu = \Gamma_e \approx 1$. The average scalar potential $\hat{\Gamma}_i\tilde{\varphi} = \hat{\Gamma}_\nu\tilde{\varphi}$ ($\nu = 1, 2, 3$) introduced in the GKZ model determines the cutting distance (δ_φ) of the parallel electric field in the vicinity of the singular surface X_S. When the local ion Larmor radius ($\rho_{xi} = \rho_{x\nu}$, $\nu = 1, 2, 3$) in the vicinity of X_S is smaller than the spatial scale of variation of the resonant ion current ($\delta_i = \delta_\nu$, $\nu = 1, 2, 3$), the operator $\hat{\Gamma}_i$ can be expanded as $\hat{\Gamma}_i \approx 1 - \rho_{xi}^2\hat{k}_x^2/2$, and the quasi-neutrality equation (37) takes the differential form

$$\frac{1}{2}\rho_{ix}^2\zeta_i\left(W_{i0}\frac{d^2\tilde{\varphi}}{dX^2} - \frac{v_{Ti}}{c}W_{i1}\frac{d^2A_1}{dX^2}\right) = \left(\tilde{\varphi} - \frac{\bar{\omega}_\nu}{k_\| c}A_1\right)(\zeta_i W_{i0} + 1) \tag{41}$$

where

$$W_{in} = \sum_{\nu=1}^{3} W_{\nu n} \approx \frac{\omega - \omega_i^* - \omega_E}{\bar{\omega}_i} Z_n(\zeta_i)$$

$\zeta_i = \zeta_\nu$ and $\bar{\omega}_i - \bar{\omega}_\nu$ for $\nu = 1, 2, 3$.

The parallel Ampere's law (35) (where $\hat{V}A_1$ is given by (38)) together with the quasi-neutrality condition (41) form a set of two coupled second-order differential equations, which constitutes the eigenvalue problem for the collisionless drift tearing mode when $\rho_{xi} \ll \delta_i$. The similar system for the symmetrical Harris equilibrium (when all coefficients in the differential equations can be expressed analytically) was solved by *Gladd* [1990] with the use of an integration scheme utilizing Ricatti transforms. The numerical growth rates were found to be smaller than analytical estimates given by the GKZ model, while there was no disagreement on the parametric dependences of the stability thresholds. The main purpose of this paper is to analyze the modifications of the stability thresholds due to asymmetries in the magnetic field profile. We assume that after the instability onset the linear collisionless growth rate could be modified, for instance, due to coupling with high-frequency electrostatic turbulence or due to overlapping of nearby growing magnetic islands. Therefore we will apply the "A_1 = const" approximation used in the GKZ model and neglect the term proportional to the operator $\hat{R}_i$ in (38).

In the GKZ model it was illustrated that the condition $\rho_{xi} \ll \delta_i$ is very rarely satisfied within the typical MCL. It is more appropriate to consider the opposite case $\rho_{xi} > \delta_i$ when the operator $\hat{\Gamma}_i$ and, consequently, the quasi-neutrality equation (37) take an integral form. Evaluation of the solution of the quasi-neutrality equation in this "integral" case was presented in the paper by *Galeev et al.* [1986]. In the next section we will neglect unimportant logarithmic corrections ("residual" ion magnetization in the region $|x| < \rho_{xi}$) and use the approximate "steplike" expressions for the perturbed electrostatic potential and for the operator $\hat{\Gamma}_i$

$$\tilde{\varphi} = \frac{\bar{\omega}_i}{k_\| c}\hat{h}(|x| - \delta_i)A_1, \quad \hat{\Gamma}_i = \hat{h}(|x| - \rho_{xi}), \quad \rho_{xi} > \delta_i \tag{42}$$

where $\hat{h}(\xi)$ is the Heaviside step function.

5 Criterion of a magnetic surface stability

The dispersion relation in "A_1 =const" approximation acquires the following form (see, for example, *Galeev and Zelenyi* [1977]):

$$\Delta' = \frac{1}{2}\int_{-\infty}^{\infty} \hat{V}\, dX = U_e + U_i \tag{43}$$

The right-hand side of (43) is a total nonadiabatic response which is proportional to the perturbed electric field work upon the singular current. The term U_e describes the irreversible increase of resonant electron energy, while U_i is the energy expenditure for the excitation of field-aligned ion oscillations. The values of these integrals are controlled by the local values of the magnetic field and electron density in the region of the singular surface $X = X_S$ and can be estimated from (38) where the term proportional to $\hat{R}_i$ is neglected, and $\hat{\Gamma}_i\tilde{\varphi}$ is expressed through A_1 with the help of (42)

$$U_e \approx -\imath\pi^{1/2}\frac{2\omega_{pe}^2}{c^2}\frac{(\omega - \omega_e^* - \omega_E)}{k_\parallel' v_{Te}} \tag{44}$$

$$U_i \approx \frac{2\omega_{pi}^2}{c^2}\frac{(\omega - \omega_i^* - \omega_E)}{k_\parallel' v_{Ti}}\frac{\delta_i}{\rho_{xi}} \tag{45}$$

The solution of the dispersion equation (43) for the drift tearing mode $\omega = \omega_r + \imath\gamma$ ($\omega_r \gg \gamma$) takes the form

$$\omega_r \approx \omega_e^* + \omega_E(X_S) = -\frac{cT_e k B_z(X_s)}{eB_1 B(X_S) D}\frac{n_4(X_S)}{n(X_S)} \tag{46a}$$

$$\gamma \approx \gamma_L(1 - a) \tag{46b}$$

where $\gamma_L = \Delta' c^2 k_\parallel' v_{Te}/\omega_{pe}^2(X_S)\sqrt{\pi}$ is the linear tearing mode growth rate. The parameter $a \approx U_i/\Delta'$ characterizes the departure of the mode from its linear stability threshold. Far from the stability threshold the growth rate is thus mainly controlled by the electrons and is positive for all parameters when Δ' is positive. The stabilizing effect is related to the coupling of tearing perturbations with field-aligned ion sound waves [*Coppi et al.*, 1979; *Galeev et al.*, 1986]. In this study, we are mainly interested in the threshold conditions when the growth rate changes its sign. When the ion term U_i becomes larger than the free energy Δ' the growth rate should change sign and the threshold ($\gamma = 0$) can be obtained from the condition

$$\Delta' = 2\frac{\omega_e^* - \omega_i^*}{k_\parallel' v_{Ti}}\eta_i\beta(X_S)\frac{\delta_i}{\rho_{xi}^3} \tag{47}$$

obtained substituting $\gamma = 0$ and $\omega = \omega_e^* + \omega_E$ in (43)–(45).

The results of the numerical solution of the dispersion equation (47) are shown on Figures 7a–7f, where the dependences of the threshold wave number $k_{cr}D$ on X_S/D for different values of θ_0, B_1, and B_2 are presented. Instability development on the magnetic

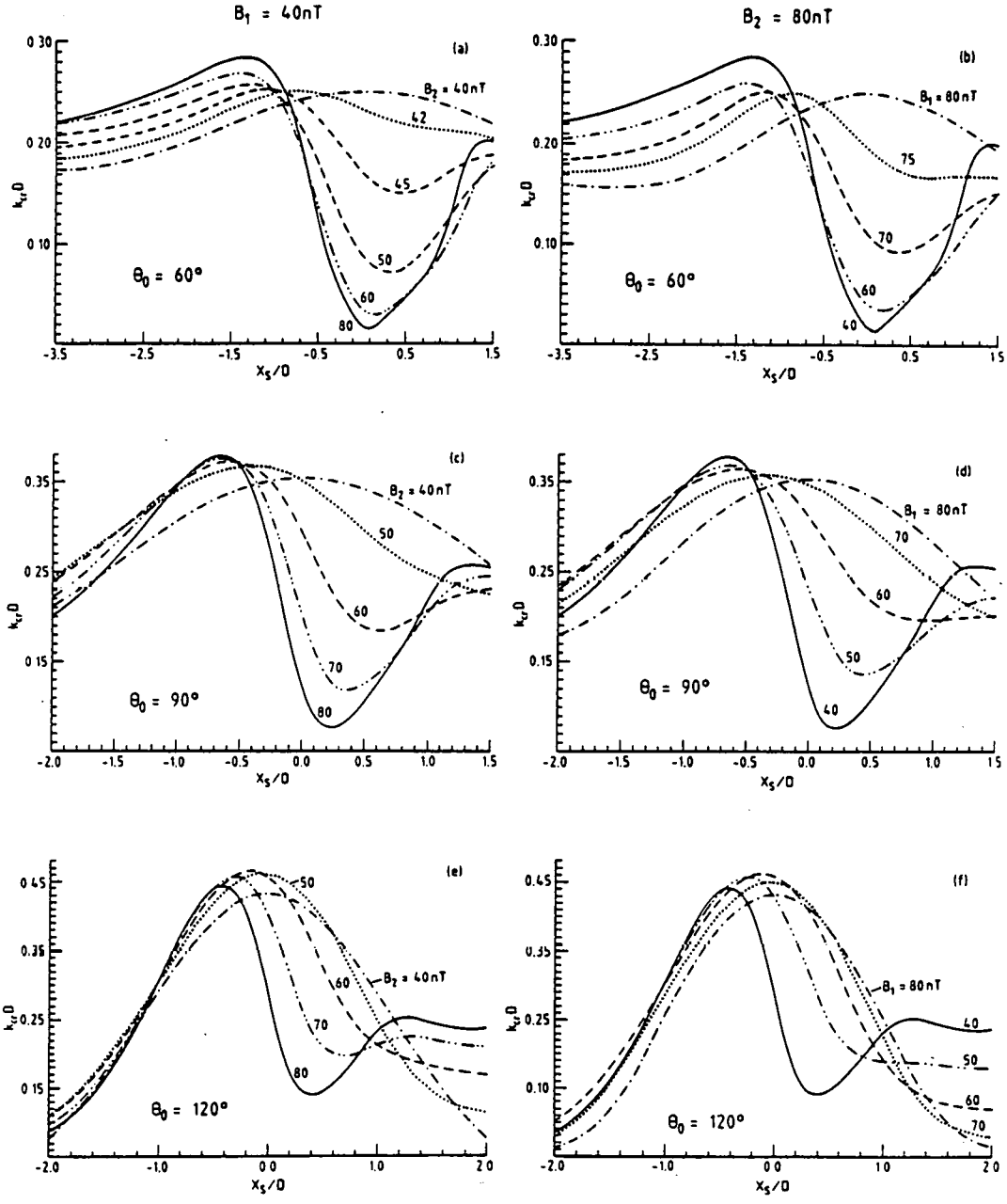

Figure 7: Threshold wave number $k_{cr}D$ as a function of X_S/D for different values of θ_0, B_1, and B_2. (left) Case 1. (right) Case 2. Instability development on the magnetic surface X_S is possible only if the perturbation wavelength λ is greater than $\lambda_{cr} = 2\pi/k_{cr}$. The dotted-dashed curves correspond to the GKZ model.

surface X_S is possible only if the perturbation wavelength λ is greater than $\lambda_{cr} = 2\pi/k_{cr}$. Perturbations with wavelengths less than λ_{cr} are completely stabilized.

It can be seen that curves in Figures 7a–7f with equal asymmetry factors but from different sets (1: $B_1 = \text{const}$, and 2: $B_2 = \text{const}$) are qualitatively similar. The maxima of the curves in Figures 7a–7f correspond to the "most unstable" magnetic surface X_S^M with the widest range of wavelengths of unstable modes. For the symmetrical case (the GKZ model represented by the dot-dashed curves) this most unstable surface is the central magnetic surface $X_S^M = 0$. For asymmetrical MCLs the most unstable surface is shifted to the magnetosheath side, the smaller θ_0 the larger the shift. For instance, for the asymmetry factor $\kappa_B = 0.5$ ($B_2 = 2B_1$; solid curves in Figures 7a–7f) the most unstable magnetic surface is shifted to $X_S^M \approx -0.5D$ for $\theta_0 = 120°$, to $X_S^M \approx -0.7D$ for $\theta_0 = 90°$, and to $X_S^M \approx -1.3D$ for $\theta_0 = 60°$. Comparing curves in Figures 7a–7f with the number density profiles shown in Figure 2 (where $D = 2\rho$), it can be seen that the maxima in corresponding curves, that is, in those with the same values of θ_0 and κ_B, are located at nearly the same X_S. This means that the most unstable magnetic surfaces are located close to the maxima of the number density profiles. Near the maximum ($X_S = X_S^M$) the stabilizing influence of the coupling with ion field-aligned oscillations appears to be inefficient. At $X = X_S^M$ the critical wavelength $(\lambda_{cr})_{min}$ is determined mainly by the free energy source of the instability, that is, from the condition $\Delta' = 0$. For the symmetrical MCL this condition corresponds to $(k_{cr})_{max}D = 0.5\sin(\theta_0/2)$, or to $(\lambda_{cr})_{min} = 4\pi D/\sin(\theta_0/2)$. In Figures 7a–7f the values of $(k_{cr})_{max}$ for asymmetrical MCLs are all systematically higher than the one for the symmetrical MCL, which means that the corresponding critical wavelengths are shorter. For the most asymmetrical MCLs, this effect is the most pronounced for $\theta_0 \leq 90°$ (especially for $\theta_0 = 60°$).

The minima of the curves in Figures 7a–7f correspond to the most stable magnetic surfaces X_S^* where the range of wavelengths of unstable modes is the most narrow, that is, only very long wave perturbations can be excited. Comparing curves in Figures 7a–7f with the number density profiles shown in Figure 2 (where $D = 2\rho$), it can be seen that the most stable magnetic surfaces X_S^* are located in regions with the strongest density gradients, where drift effects are more effective. Perturbations near the magnetic surface $X_S = X_S^*$ are strongly coupled with ion sound oscillations that carry away the wave energy from the interaction region.

For symmetrical MCLs the most stable magnetic surfaces are located symmetrically at both edges of the layers (see the dotted-dashed curves in Figures 7a–7f). For asymmetrical MCLs, Figures 7a–7f show that the stability of the magnetospheric part of the layers ($X_S > 0$) is more affected by the asymmetry of the magnetic field than the magnetosheath part ($X_S < 0$). In particular, in asymmetrical MCLs the stability of the magnetospheric part is strongly dependent on the orientation of the interplanetary magnetic field (IMF), that is, on the value of θ_0. Indeed, nearly all curves in Figures 7a–7d have a well pronounced minimum in the region $X_S > 0$, the exceptions being the dotted-dashed curves corresponding to the symmetrical case ($\kappa_B = 0$), and the dotted curves corresponding to small values of the asymmetry factor κ_B (see Table 1). This means that, when the value of κ_B is not too small, asymmetrical MCLs with $\theta_0 \leq 90°$ (corresponding to a northward orientation of the IMF) are then characterized by an internal magnetic surface at $X = X_S^*$,

inside the magnetospheric region, which is the most stable. Furthermore, when κ_B increases (keeping a fixed value for θ_0) this most stable magnetic surface (corresponding to the position of the minima in the curves ilustrated in Figures 7a–7d) "moves" deeper into the layer and the range of wavelengths for its stable modes increases (the depth of the minima in the curves illustrated in Figures 7a–7d increases).

For asymmetrical MCL's with $\theta_0 > 90°$ (Figures 7e and 7f when $\theta_0 = 120°$), the magnetospheric edge is more unstable than the magnetosheath one, since the corresponding curves in Figures 7e and 7f are above the dotted-dashed curve of the symmetrical case when $X_S \gg 0$. It is only when $\kappa_B > 0.4$ that there is a pronounced minimum in the threshold wave number curve (see the solid lines in Figures 7e and 7f corresponding to $\kappa_B = 0.5$, $B_2 = 2B_1$), similar to those found for several non-zero values of κ_B when $\theta_0 \leq 90°$ (see Figures 7a–7d).

Note that with the decrease of θ_0 (for a fixed value of κ_B) the most stable magnetic surfaces X_S^* are shifted closer to the center of the layers. For instance, for $\kappa_B = 0.5$ ($B_2 = 2B_1$, the solid curves in Figures 7a–7f), the most stable surface is at $X_S^* \approx 0.4D$ when $\theta_0 = 120°$ (Figures 7e and 7f), at $X_S^* \approx 0.2D$ when $\theta_0 = 90°$ (Figures 7c and 7df), and at $X_S^* \approx 0$ when $\theta_0 = 60°$ (Figures 7a and 7b).

6 Marginal Thickness of Asymmetrical MCLs

According to the GKZ model the necessary condition for the magnetic percolation through the MCL is the destruction of all magnetic surfaces within it (see *Galeev et al.*'s [1986], Figure 1a illustrating the stochastic wandering of magnetic field lines through the layer and the resulting magnetic percolation). If a domain with stable and smooth magnetic surfaces exists within the MCL (somewhere in the vicinity of the most stable magnetic surface X_s^*) the MCL appears to be impenetrable for the diffusing field lines (see *Galeev et al.*'s [1986], Figure 1b illustrating the interruption of the percolation process).

If all magnetic surfaces within the MCL are destroyed and the percolation is successfully accomplished the minimum excursion of the percolated field lines along the magnetopause should not be smaller than the critical wavelength for the most stable magnetic surface

$$\lambda^* = \lambda_{cr}(X_s^*) = (\lambda_{cr})_{\max}$$

It is seen from Figures 2 and 3 that all plasma and field parameters are varying on a characteristic distance of the order of

$$L_0 \approx 4D \tag{48}$$

Let us adopt this value for the characteristic thickness of the magnetopause. Thus for each D, B_1, B_2, and θ_0, we select the region $\Delta X = L_0$ where the conditions for the instability development are the most favorable, and find the magnetic surface within it characterized by the maximum critical wavelength λ^*. This critical wavelength can be identified with the minimum "latitudinal" spatial scale of the reconnection patch on the magnetopause surface.

The dependences of the dimensionless spatial scale λ^*/ρ on the dimensionless magnetopause thickness L_0/ρ for different values of θ_0 and κ_B (that is, different values of B_1 and B_2) are shown on Figure 8. The lower curves in each panel correspond to reconnection patches with the smallest spatial scale for identical MCL thickness, and correspond therefore to cases where the MCL can be easily percolated. For $\theta_0 = 60°$ the results are very sensitive to the value of the asymmetry factor, that is, even curves corresponding to very small asymmetry factors ($\kappa_B \approx 0.07$, or, case 1: $B_1 = 40$ nT, $B_2 = 43$ nT; case 2: $B_2 = 80$ nT, $B_1 = 75$ nT) are well separated from the curves corresponding to the symmetrical case (case 1: $B_1 = B_2 = 40$ nT; case 2: $B_1 = B_2 = 80$ nT). For $\theta_0 = 90°$ and $\theta_0 = 120°$ the dependence on κ_B is less pronounced. Therefore, in addition to the curves corresponding to the symmetrical case ($\kappa_B = 0$) only curves corresponding to $\kappa_B \geq 0.2$ are displayed when $\theta_0 \geq 90°$. It is seen that for $\theta_0 = 120°$ the curves corresponding to different asymmetry factors are much closer to each other (that is, less sensitive to the value of κ_B) than for $\theta_0 = 90°$. For $\theta_0 = 60°$ and $\theta_0 = 90°$ the largest asymmetry factors κ_B correspond to the largest spatial scales λ^*. For the latter values of θ_0, the symmetrical case ($B_1 = B_2 = 40$ nT in the left column, $B_1 = B_2 = 80$ nT in the right column) is seen to correspond to the lowest values of λ^*/ρ, and is therefore the most favorable case for percolation. However, when $\theta_0 = 120°$, it can be seen that the symmetrical case is not the most favorable case for percolation. Indeed, for $\theta_0 = 120°$, the lowest curve corresponds to $B_1 = 40$ nT and $B_2 = 70$ nT in the left column (case 1), and to $B_1 = 50$ nT and $B_2 = 80$ nT in the right column (case 2). Therefore, for large angles $\theta_0 \approx 120°$, the most favorable configurations for percolation are asymmetrical configurations with asymmetry factors κ_B of the order of 0.4.

One can assume that the characteristic spatial scale along the magnetopause λ_{ext} is determined by the external conditions (the size of the magnetopause, the convection pattern in the magnetosheath). Let us assume that $\lambda_{ext} = 90\rho \approx 10{,}000$ km. The dependence of the dimensionless marginal magnetopause thickness L_0^{cr}/ρ on θ_0 for different κ_B is shown on Figures 9a and 9b. A MCL of thickness less than the marginal one (L_0^{cr}) will be subjected to percolation of magnetic field lines. The results shown on Figures 9a and 9b can be considered as the generalization of the GKZ model for the asymmetrical case.

Note that the characteristic thickness L_0^{GKZ} used in the GKZ model ($L_0^{GKZ} = 2L$) is linked to the characteristic thickness L_0 used in the present study by the relation $L_0/L_0^{GKZ} = \sin(\theta_0/2)$ (see equations (13) and (48)). In the GKZ model, the "most favorable angle for percolation" θ_0^* (corresponding to the maximum marginal thickness L_0^{cr}) depends on the definition of the MCL thickness and on the parameter α (see equation (3)), but its value was always found less than 90° (that is, in symmetrical MCLs, θ_0^* was always found to correspond to a northward orientation of the IMF). For instance, in *Galeev et al.* [1986, Figure 5] $\theta_0^* \approx 60°$, for a thickness definition given by (13) and $\alpha = 1$. For a thickness definition given by (48) and $\alpha = 0$, the most favorable angle for percolation in symmetrical MCLs is $\theta_0^* \approx 85°$ (see curves corresponding to symmetrical configurations in Figures 9a and 9b).

Despite the fact that the series of curves in Figure 9a and 9b are qualitatively similar to each other, it can be seen that in case 2 (when the magnetic field is kept constant

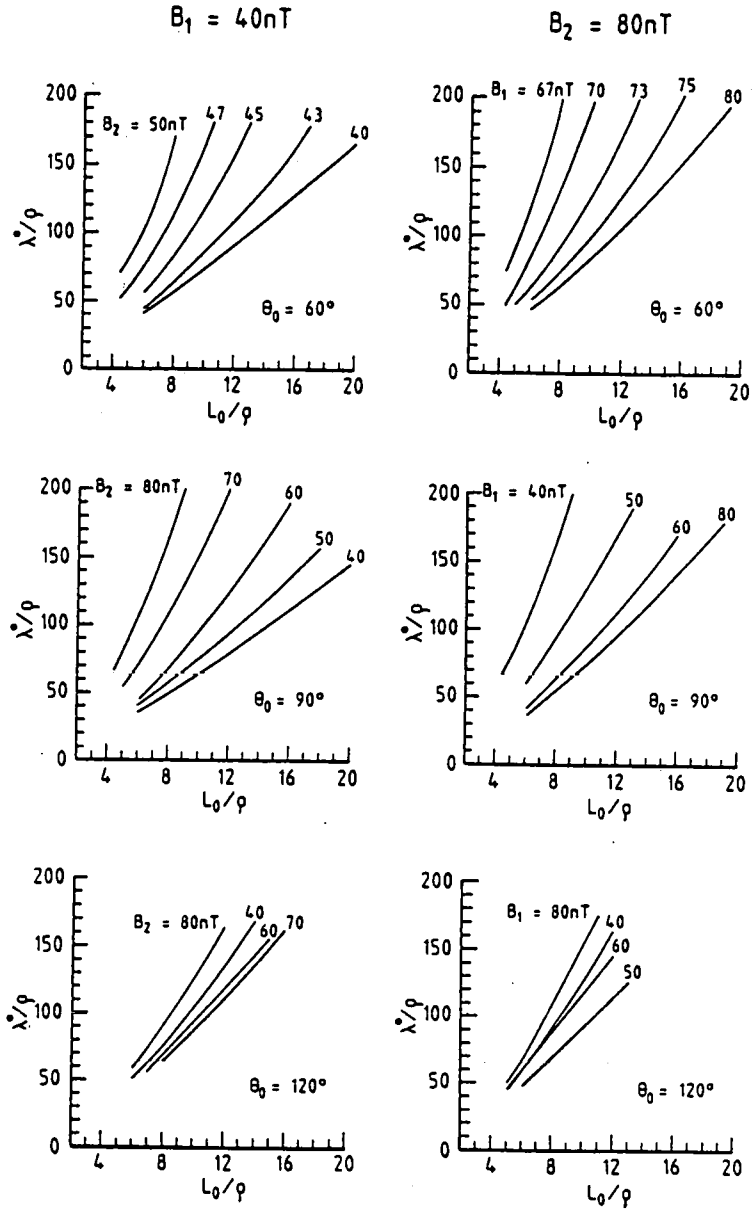

Figure 8: Dimensionless minimum spatial scale of the reconnection patch λ^*/ρ as a function of the dimensionless MCL thickness $L_0/\rho = 4D/\rho$ for different values of B_1, B_2 and θ_0. (left) Case 1. (right) Case 2. It can be seen that for $\theta_0 = 60°$ and $\theta_0 = 90°$, the symmetrical case ($B_1 = B_2 = 40$ nT in the left column, $B_1 = B_2 = 80$ nT in the right column) corresponds to the lowest value of λ^*/ρ, and represents therefore the most favorable case for percolation. For $\theta_0 = 120°$, asymmetrical configurations with asymmetry factors κ_B of the order of 0.4 represent however the most favorable configurations for percolation.

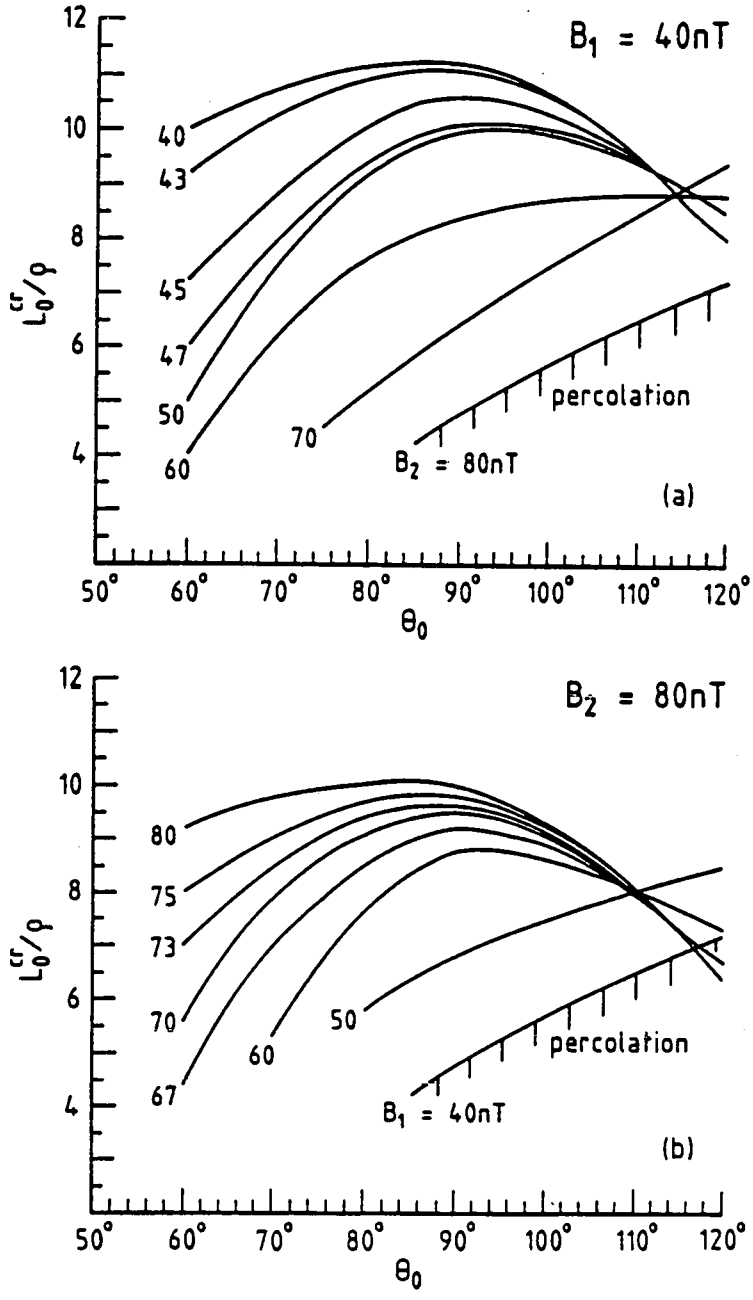

Figure 9: Dimensionless marginal magnetopause thickness L_0^{cr}/ρ as a function of θ_0 for different values of B_1 and B_2, and assuming that the spatial scale of the reconnection patch $\lambda_{ext} = 90\rho \approx$ 10,000 km (ρ is the Larmor radius of a ion with a typical thermal energy of 1 keV, in a magnetic field intensity of 40 nT, $\rho = 114.3$ km). (a) The magnitude of the magnetic field in the adjacent magnetosheath region is fixed, B_1=40 nT, while the intensity of the magnetospheric field (B_2) is changing from 40 nT to 80 nT (case 1). (b) The magnitude of the magnetic field in the adjacent magnetospheric region is fixed, B_2=80 nT, while the intensity of the magnetic field in the adjacent magnetosheath (B_1) is changing from 80 to 40 nT (case 2).

on the magnetospheric side) the marginal thickness is more sensitive to the value of the asymmetry factor than in case 1 (when the magnetic field is kept constant on the magnetosheath side). The introduction of the asymmetry in the magnetic field profile significantly modifies the dependence of the marginal MCL thickness on the angle of the magnetic field rotation θ_0. When $\theta_0 < 90°$, it can be seen that even for small values of the asymmetry factor ($\kappa_B \geq 0.15$) the marginal thickness L_0^{cr} is significantly decreased, that is, only thin MCLs can be subjected to percolation. Furthermore, for very asymmetrical MCLs ($\kappa_B \geq 0.4$) with $\theta_0 < 90°$ (northward IMF) the percolation becomes impossible. Therefore the most favorable angle for percolation (θ_0^*) is shifted to larger values: $\theta_0^* > 90°$ (southward IMF). The larger the asymmetry factor κ_B, the larger the angle θ_0^*. For very asymmetrical MCLs ($\kappa_B \geq 0.4$), $\theta_0^* \geq 120°$.

If the magnetopause thickness is much larger than the marginal one a large domain of stable magnetic surfaces should exist within it which should prevent particles diffusion across the layer. In this case a one-dimensional slab TD could be considered as a good approximation for the magnetopause current layer if one disregards the question of particle accessibility both in the current layer itself, and more specifically to different phase space regions. However, consideration of particle accessibility in Vlasov theories of plane TD's requires the knowledge of the characteristics of the plasma in the source regions together with the transport mechanisms bringing the plasma to the transition itself [*Whipple et al.*, 1984]. In the opposite case, that is, when the magnetopause thickness is much less than the marginal one, the strong large-scale magnetic turbulence developing within the layer should result in turbulent reconnection and current sheet broadening. A diffusive broadening of the symmetrical current layer when a large number of tearing modes are allowed to grow together was illustrated by *Wang and Ashour-Abdalla* [1994] using a three-dimensional particle simulation.

Thus it is reasonable to assume that the magnetopause thickness should, on the average, tend to the marginal one. The magnetopause current layer in this case could be modeled as a one-dimensional tangential discontinuity perturbed by embedded percolated magnetic filaments. From this point of view, curves in Figures 9a and 9b represent a characteristic dependence of the magnetopause thickness on the angle θ_0. It is seen that in realistic asymmetrical cases ($\kappa_B > 0.3$) the magnetopause should be thinner for $\theta_0 < 90°$ (northward IMF) than for $\theta_0 > 90°$ (southward IMF).

7 Summary and Conclusions

The aim of this study has been to understand some of the basic signatures of the internal structure of the magnetopause current layer (MCL) when the latter is not an electrostatically equipotential configuration and is characterized by an asymmetrical magnetic field profile. Within such MCLs we have investigated the stability of magnetic surfaces with respect to spontaneous excitation of collisionless tearing perturbations. The stochastic percolation model by *Galeev et al.* [1986] (the GKZ model), based on the symmetrical equilibrium configuration of Harris, has been reconsidered and generalized.

In this study, two groups of Vlasov equilibrium configurations have been considered.

The first one (referred to as case 1) corresponds to situations when an increase of the kinetic pressure in the magnetosheath (B_1 fixed) caused an earthward displacement of the MCL (B_2 is increasing, N_2 is fixed). The second group (referred to as case 2) corresponds to situations where the positions of the MCLs are fixed (B_2 and N_2 are fixed), while any increase of the kinetic pressure in the adjacent magnetosheath results in a corresponding reduction of the magnetic pressure (B_1 is decreasing). In both groups, the internal structure of the MCL depends on two parameters characterizing the magnetic field asymmetry, that is, the asymmetry factor ($\kappa_B = (B_2 - B_1)/B_2$) and the angle of rotation of the magnetic field (θ_0). These parameters determine in particular the plasma density and the magnetic field in the center of the layer. We have shown that the number density in the center of the MCL strongly depends on the magnetic field asymmetry parameters for MCLs of group 1, but is rather insensitive to these parameters for MCLs of group 2. The magnetic field asymmetry significantly modifies the B_y and J_z profiles (with respect to the symmetrical Harris case), while the B_z and J_y profiles are only slightly affected. This means that the asymmetry is mainly controlled by the magnetosheath and magnetospheric ions and not by the trapped particles. Moreover, the electric field distribution is strongly dependent on the magnetic field asymmetry, and the departure from the equipotential condition, $\phi(X)$=const, is already significant for rather small values of κ_B. Note that the introduction of the asymmetry in our model leads to the increase of the plasma beta in the magnetosheath, from nearly zero (for $\kappa_B \to 0$) to $2 \div 3$ (for $\kappa_B > 0.3$).

The modifications of the initial symmetrical Harris configuration (1), introduced by the presence of an asymmetrical magnetic field profile, strongly influence the adiabatic interaction of the plasma with tearing-type perturbations as well as the nonadiabatic response of the particles near the center of the MCL. In other words, the free energy of the perturbations (controlled by the global plasma and field distributions) and the singular current (controlled by the local values of the plasma density and magnetic field near the center of the MCL) are both significantly modified by the presence of a magnetic field asymmetry. Configurations with the largest degree of asymmetry κ_B have the largest excess of free energy Δ' and are thus potentially more unstable than the symmetrical ones. The stabilizing effect related to the coupling of tearing perturbations with field-aligned ion sound waves has also been studied.

For asymmetrical MCLs the most unstable magnetic surfaces (those with the widest range of wavelengths for unstable modes) are no longer located at $X = 0$ as in the GKZ model but are shifted to the magnetosheath side. This shift is more pronounced for small values of the magnetic field rotation. The most unstable magnetic surfaces are located close to the maxima of the number density profiles. Near these most unstable magnetic surfaces, the stabilizing influence of the coupling with ion field-aligned oscillations appears to be inefficient and the threshold wave number is mainly determined by the free energy source of the instability. The most stable magnetic surfaces are located in regions with the strongest density gradients, where drift effects are more effective. Perturbations near these most stable magnetic surfaces are strongly coupled with ion sound oscillations that carry away the wave energy from the interaction region. For a northward orientation of the IMF ($\theta_0 \leq 90°$) the magnetospheric edge of the asymmetrical MCL has been found to be more stable than the magnetosheath one. With the increase of κ_B, the most stable

(magnetospheric) surfaces (that is, those where the range of wavelengths of unstable modes is the most narrow) move deeper into the layer and the range of wavelengths for their stable modes still increases. For a southward orientation of the IMF ($\theta_0 > 90°$), a moderate asymmetry ($\kappa_B \leq 0.4$) makes the magnetospheric part of the MCL more unstable. A region with a most stable magnetic surface is present in the magnetospheric part only for very asymmetrical MCLs ($\kappa_B > 0.4$).

According to the GKZ model, almost all the magnetic surfaces within the magnetopause layer must be unstable to accomplish the percolation process. The characteristic spatial scale of the reconnection patch λ_{ext} is limited internally from below by the conditions of the tearing-mode destabilization and growth: $\lambda_{ext} > \lambda^* = \lambda_{cr}(X_S^*) = (\lambda_{cr})_{max}$. The external conditions of plasma motion within the magnetosheath impose the other upper boundary: $\lambda_{ext} < 1\text{–}2R_E$. A typical value of λ_{ext} has been chosen of the order of 90 ρ, that is, $\lambda_{ext} \approx$ 10,000 km. For $\theta_0 = 60°$ and $\theta_0 = 90°$, the symmetrical case ($B_1 = B_2$) corresponds to the lowest value of λ^* and therefore represents the most favorable case for percolation, However, for $\theta_0 = 120°$, asymmetrical MCLs appear to be more unstable, the most favorable ones for percolation having asymmetry factors κ_B of the order of 0.4.

The introduction of asymmetry in the magnetic field profile strongly modifies the dependence of the marginal MCL thickness (below which the MCL is subjected to percolation) on the polarity of the interplanetary magnetic field (IMF). In the GKZ model, a northward orientation of the IMF was found to be optimum for percolation, that is, the maximum thickness of Harris-type layers subjected to percolation is achieved for $\theta_0 < 90°$. The introduction of asymmetry in the magnetic field helps to overcome this seemingly contradiction with experimental data [*Berchem and Russel*, 1984; *Southwood et al.*, 1986]. It is demonstrated that for $\theta_0 < 90°$, and especially when the magnetospheric field B_2 is kept constant (MCLs of group 2), the marginal thickness is significantly smaller than that computed in the GKZ model, even for small values of κ_B. This means that for $\theta_0 < 90°$ only thin asymmetrical MCLs can be subjected to percolation. For very asymmetrical MCLs ($\kappa_B \geq 0.4$) the percolation is possible only for $\theta_0 > 90°$, that is, for a southward IMF polarity (with $\theta_0 \geq 120°$ the optimum range for percolation).

Assuming that the magnetopause should, on the average, be close to the threshold of its stability it is found that realistic asymmetrical MCLs (with $\kappa_B > 0.3$) should be thinner for a northward IMF than for a southward IMF.

When the threshold conditions for percolation are satisfied the magnetic field lines become stochastic. In symmetrical charge-neutral MCLs composed of trapped particles, the field line stochasticity can only result in a diffusive broadening of the current layer. The formation of percolated magnetic filaments in asymmetrical MCLs should result in a diffusive penetration of particles from the magnetosheath to the magnetosphere, that should be accompanied by particle heating. It is also interesting to consider the role of the equilibrium electric field which, after percolation, has a component parallel to the magnetic filament. This parallel electric field component should provide the MCL with the feature of a "semipermeable membrane" at the early stage of diffusion. Indeed, the potential drop across the asymmetrical MCL ($\sim$ 700 V) will accelerate the magnetosheath ions and prevent the cold magnetospheric ions to overcome the potential barrier. However, magnetic field line stochasticity and particle diffusion in asymmetrical, electrostatically non

equipotential MCLs represent important challenging problems that should be attacked by methods of particle simulation.

Acknowledgments

The authors would like to thank L. Zelenyi and J. Lemaire for permanent interest in this work. M.M.K. is grateful to M. Ashour-Abdalla and B. U. Ö. Sonnerup for discussions and valuable comments. M.R. thanks the National Fund for Scientific Research (Belgium) for a research grant. We are also grateful to M. Ackerman, Director of the Belgian Institute for Space Aeronomy, for his permanent support.

The Editor thanks two referees for their assistance in evaluating this paper.

(Received December 21, 1993; revised July 6, 1994; accepted August 30, 1994).

References

Alpers, W., Steady state charge neutral models of the magnetopause, *Astrophys. Space Sci., 5*, 425, 1969.

Berchem, J., and C.T. Russell, Flux transfer events on the magnetopause. spatial distributions and controlling factors, *J. Geophys. Res., 89*, 6689, 1984.

Bryant, D.A., and S. Riggs, At the edge of the Earth's magnetosphere: a survey by AMPTE-UKS, *Philos. Trans. R. Soc. London Ser. A, 328*, 43, 1989.

Coppi, B., J.W.-K. Mark, L. Sugiyama, and G. Bertin, Reconnecting modes in collisionless plasmas, *Phys. Rev. Lett., 42*, 1058, 1979.

Ding, D.Q., L.C. Lee, and Z.W. Ma, Different FTE signatures generated by the bursty single X line reconnection and the multiple X line reconnection at the dayside magnetopause, *J. Geophys. Res., 96*, 57, 1991.

Ding, D.Q., L.C. Lee, and C.F. Kennel, The beta dependence of the collisionless tearing instability at the dayside magnetopause, *J. Geophys. Res., 97*, 8257, 1992a.

Ding, D.Q., L.C. Lee, and D.W. Swift, Particle simulations of driven collisionless magnetic reconnection at the dayside magnetopause, *J. Geophys. Res., 97*, 8453, 1992b.

Drake, J.F., and Y.C. Lee, Kinetic theory of tearing instabilities, *Phys. Fluids, 20*, 1341, 1977.

Drake, J.F., T.M. Antonsen Jr., A.B. Hassam, and N.T. Gladd, Stabilization of the tearing mode in high temperature plasmas, *Phys. Fluids, 26*, 2509, 1983.

Drake, J.F., J. Gerber, and R.G. Kleva, Turbulence and transport in the magnetopause current layer, *J. Geophys. Res., 99*, 11,211, 1994a.

Fu, Z.F., and L.C. Lee, Simulation of multiple X–line reconnection at the dayside magnetopause, *Geophys. Res. Lett., 12*, 291, 1985.

Fu, Z.F., L.C. Lee, and Y. Shi, A three-dimensional MHD simulation of the multiple X line reconnection process, in *The Physics of Magnetic Flux Ropes, Geophys. Monogr. Ser.*, vol. 58, edited by C.T. Russell, E.R. Priest, and L.C. Lee, p. 515, AGU, Washington, D. C., 1990.

Furth, H.P., J. Killeen, and M.N. Rosenbluth, Finite-resisti-vity instabilities in a sheet pinch, *Phys Fluids, 6*, 459, 1963.

Galeev, A.A., and L.M. Zelenyi, The model of magnetic field reconnection in a slab collisionless plasma sheath, *Pis'ma Zh. Eksp. Teor. Fiz., 25*, 407, 1977.

Galeev, A.A., M.M. Kuznetsova, and L.M. Zelenyi, Magnetopause stability threshold for patchy reconnection, *Space Sci. Rev., 44*, 1, 1986.

Gary, S.P., and T. E. Eastman, The lower hybrid drift instability at the magnetopause, *J. Geophys. Res., 84*, 7378, 1979.

Gary, S.P., and A.G. Srgo, The lower hybrid drift instability at the magnetopause, *Geophy. Res. Lett., 17*, 909, 1990.

Gladd, N.T., Collisionless drift-tearing modes in the magnetopause, *J. Geophys. Res., 95*, 20,889, 1990.

Gladd, N.T., A.G. Sgro, and D.W. Hewett, Microstability properties of the sheath region of a field reversed configuration, *Phys. Fluids, 28*(7), 2222, 1985.

Gurnett, D.A., R.R. Anderson, B.T. Tsurutani, E.J. Smith, G.Paschmann, G. Haerendal, S.J. Bame, and C.T. Russell, Plasma wave turbulence at the magnetopause: Observations from ISEE 1 and 2, *J. Geophys. Res., 84*, 7043, 1979.

Harris, E.G., On a plasma sheath separating regions of oppositely directed magnetic field, *Nuovo Cimento, 23*, 115, 1962.

Hesse, M., J. Birn, and K. Schindler, On the topology of flux transfer events, *J. Geophys. Res., 95*, 6549, 1990.

Hoshino, M., and A. Nishida, Numerical simulation of the dayside reconnection, *J. Geophys. Res., 88*, 6926, 1983.

Huba, J.B., N.T. Gladd, and J.F. Drake, The lower hybrid drift instability in non-antiparallel reversed field plasmas, *J. Geophys. Res., 87*, 1697, 1982.

Kan, J.R., Equilibrium configurations of Vlasov plasmas carrying a current component along an external magnetic field, *J. Plasma Phys., 7*, 445, 1972.

Krall, N.A., Shear stabilization of lower hybrid drift instabilites, *Phys. Fluids, 20*, 311, 1977.

Kuznetsova, M.M., and L.M. Zelenyi, Stability and structure of the perturbations of the magnetic surfaces in the magnetic transitional layers, *Plasma Phys. Controlled Fusion, 27*, 363, 1985.

Kuznetsova, M.M., and L.M. Zelenyi, The theory of FTE stochastic percolation model, in *Physics of Magnetic Flux Ropes*, Geophys. Monogr. Ser., vol. 58, edited by C.T. Russel, E.R. Priest, and L.C. Lee, p. 473, AGU, Washington, D. C., 1990a.

Kuznetsova, M.M., and L.M. Zelenyi, Nonlinear evolution of magnetic island in a sheared magnetic field with uniform plasma background, *Plasma Phys. Controlled Fusion, 32*, 1183, 1990b.

Kuznetsova, M.M., M. Roth, Z. Wang, and M. Ashour-Abdalla, Effect of the relative flow velocity on the structure and stability of the magnetopause current layer, *J. Geophys. Res., 99*, 4095, 1994.

LaBelle, J., and R.A. Treumann, Plasma waves at the dayside magnetopause, *Space Sci. Rev., 47*, 175, 1988.

La Belle-Hamer, A.L., Z.F. Fu, and L.C. Lee, A mechanism for patchy reconnection at the dayside magnetopause, *Geophys. Res. Lett., 15*, 152, 1988.

Lakhina, G.S., and K. Schindler, Tearing modes in the magnetopause current sheet, *Astrophys. Space Sci., 97*, 421, 1983.

Laval, G., R. Pellat, and M. Vuillemin, Instabilités electromagnétiques des plasmas sans collisions, *Plasma Phys. Controlled Fusion Res., 2*, 259, 1966.

Lee, L.C., and Z.F. Fu, A theory of magnetic flux transfer at the Earth's magnetopause, *Geophys. Res. Lett., 12*, 105, 1985.

Lee, L.C., and J.R. Kan, A unified kinetic model of the tangential magnetopause structure, *J. Geophys. Res., 84*, 6417, 1979.

Lee, L.C., Z.W. Ma, Z.F. Fu, and A. Otto, Topology of magnetic flux ropes and formation of fossil flux transfer events and boundary layer plasmas, *J. Geophys. Res., 98*, 3943, 1993.

Lemaire, J., and L.F. Burlaga, Diamagnetic boundary layers: A kinetic theory, *Astrophys. Space Sci., 45*, 303, 1976.

Lemaire, J., and M. Roth, Non-steady-state solar wind-magnetosphere interaction, *Space Sci. Rev., 57*, 59, 1991.

Liu, Z.X., Z.W. Zhu, F. Li, and Z.Y. Pu, Topology and signatures of a model for flux transfer events based on vortex-induced reconnection, *J. Geophys. Res., 97*, 19351, 1992.

Ogino, T., R. J. Walker, and M. Ashour-Abdalla, A magnetohydrodynamic simulation of the formation of magnetic flux tubes at the Earth's dayside magnetopause, *Geophys. Res. Lett., 16*, 155, 1989.

Otto, A., 3-D resistive MHD computations of magnetospheric physics, *Comput. Phys. Commun., 59*, 185, 1990.

Press, W.H., B.P. Flannery, S.A. Teukolsky, and W.T. Vetterling, *Numerical Recipes, The Art of Scientific Computing*, Cambridge University Press, New York, 1986.

Pu, Z. Y., P.T. Hou, and Z.X. Liu, Vortex-induced tearing mode instability as a source of flux transfer events, *J. Geophys. Res., 95*, 18861, 1990.

Pudovkin, M.I., and V.S. Semenov, Magnetic field reconnection theory and the solar wind-magnetosphere interaction: A review, *Space Sci. Rev., 41*, 1, 1985.

Quest, K.B., and F.V. Coroniti, Tearing at the dayside magnetopause, *J. Geophys. Res., 86*, 3289, 1981.

Ralston, A., and H.S. Wilf, *Méthodes Mathématiques pour Calculateurs Arithmétiques*, Dunod, Paris, 1965.

Roth, M., Structure of tangential discontinuities at the magnetopause: the nose of the magnetopause, *J. Atmos. Terr. Phys., 40*, 323, 1978.

Roth, M., A microscopic description of interpenetrated plas-ma regions, in Magnetospheric Boundary Layers, edited by B. Battrick, and J. Mort, *Eur. Space Agency Spec. Publ., SP-148*, 295, 1979.

Roth, M., La structure interne de la magnétopause, *Mem. Cl. Sci. Acad. R. Belg. Collect. 8°, 44*(7), 222 pp., 1984.

Roth, M., On impulsive penetration of solar wind plasmoids into the geomagnetic field, *Planet. Space Sci., 40*, 193, 1992.

Russell, C.T., and R.C. Elphic, Initial ISEE magnetometer results: magnetopause observations, *Space Sci. Rev., 22*, 681, 1978.

Russell, C.T., and R.C. Elphic, ISEE observations of flux transfer events at the dayside magnetopause, *Geophys. Res. Lett., 6*, 33, 1979.

Sato, T., T. Shimada, M. Tanaka, T. Hayashi, and K. Watanabe, Formation of field-twisting flux tubes on the magnetopause and solar wind particle entry into the magnetosphere, *Geophys. Res. Lett., 13*, 801, 1986.

Scholer, M., Magnetic flux transfer at the magnetopause based on single X line bursty reconnection, *Geophys. Res. Lett., 15*, 291, 1988.

Scholer, M., Asymmetric time-dependent and stationary magnetic reconnection at the dayside magnetopause, *J. Geophys. Res., 94*, 15099, 1989.

Sestero, A., Structure of plasma sheaths, *Phys. Fluids, 7*, 44, 1964.

Sestero, A., Vlasov equation study of plasma motion across magnetic fields, *Phys. Fluids, 9*, 2006, 1966.

Shi, Y., and L.C. Lee, Structure of the reconnection layer at the dayside magnetopause, *Planet. Space Sci., 38*, 437, 1990.

Shi, Y., C.C. Wu, and L.C. Lee, A study of multiple X line reconnection at the dayside magnetopause, *Geophys. Res. Lett., 15*, 295, 1988.

Sibeck, D.G., Transient events in the outer magnetosphere: Boundary waves or flux transfer events?, *J. Geophys. Res., 97*, 4009, 1992.

Sotnikov, V.I., V.D. Shapiro, and V.I. Shevchenko, On the nonlinear theory of current instability of short-wave drift oscillations, *Physica D Amsterdam, 2*, 170, 1981.

Southwood, D.J., M.A. Saunders, M.W. Dunlop, W.A.C. Mier-Jedrzejowicz, and R.P. Rijnbeek, A survey of flux transfer events recorder by the UKS spacecraft magnetometer, *Planet. Space Sci., 34*, 1349, 1986.

Tetreault, D., Turbulent relaxation of magnetic fields, 2, Self-organization and intermittency, *J. Geophys. Res., 97*, 8541, 1992.

Tsurutani, B.T., A.L. Brinca, E.J. Smith, R.T. Okida, R.R. Anderson, and T.E. Eastman, A statistical study of ELF-VLF plasma waves at the magnetopause, *J. Geophys. Res., 94*, 1270, 1989.

Wang, Z., and M. Ashour-Abdalla, Topological variation in the magnetic field line at the dayside magnetopause, *J. Geophys. Res., 97*, 8245, 1992.

Wang, Z., and M. Ashour-Abdalla, Magnetic field line stochasticity at the magnetopause, *J. Geophys. Res., 99*, 2321, 1994.

Whipple E.C, J.R. Hill, and J.D. Nichols, Magnetopause structure and the question of particle accessibility, *J. Geophys. Res., 89*, 1508, 1984.